

POLITECNICO DI TORINO

Corso di Laurea Magistrale

in Ingegneria Meccanica (Mechanical Engineering)

Tesi di Laurea Magistrale

Design of a test rig for the performance evaluation of violin acoustics



Relatore

Prof. Elvio Bonisoli

Prof. Marco Casazza

Dr. Domenico Lisitano

Candidato

Sacha Turi

Anno Accademico 2019/2020

Index

Index.....	3
Abstract	4
Acknowledgement	5
1. Introduction: the bowed string state of the art	6
1.1 Helmholtz theory and concept of ideal string	6
1.2 Bow force limits in a real case: the Schelleng diagram	7
1.3 Influence of the bow acceleration: the “attack”	8
1.4 Acceptable bowing parameters values	9
1.5 Influence of the bow velocity: uncertainty on Schelleng lower bow force limit.....	10
2. Test rig design introduction	12
2.1 Bowing machines state of the art	12
2.2 String-Bow static loading condition	17
2.2.1 Constant vertical load.....	17
2.2.2 Constant external torque	19
3. Test rig realization	22
3.1 Bowing linear machine solution proposed by Festo	22
3.2 Alternative bow frog design analysis.....	24
4. Frame capture technique for bow velocity evaluation	31
Conclusions.....	36
Appendix.....	37
Reference	53

Abstract

This project of thesis aims to the analysis of different design solutions of a test rig for the performance evaluation of violin acoustics. The physics of the bowed string has been deeply analysed in history of acoustic, from different points of view; in the first part many theories spanning from 1863 to 2009 will be presented, each of them with their key points useful for the development of the subject herein presented. In the second part, the state of the art will be extended with the analysis of different bowing machines, both mechanical and computer controlled, which were of inspiration for the design choices made. In the third part, two solutions will be presented: the first one about a project of a complete linear bowing machine moved by an electric stepper motor and the second one on an alternative design of the violin's bow frog (handle) for the adaptation of acceleration sensors. In the fourth and last part, a technique for visually capturing the movement of the bow through a Matlab script will be deepened, and the results coming from real test will be presented.

Acknowledgement

The first and biggest thanks go to the main supervisor of this work of thesis, Prof. Elvio Bonisoli of the DIMEAS (Department of Mechanical and Aerospace Engineering in Polytechnic of Turin) for giving me the opportunity of deepening this very multidisciplinary and interesting subject, his infinite patience, for providing the Matlab script from his work on the Levitron, and for managing the realization of the frog device during the difficult COVID period.

Many thanks to Dr. Domenico Lisitano at DIMEAS for his constant availability and support throughout every step of this work.

Prof. Marco Casazza, violinist and professor at “Parthenope” University of Naples (in the department of Environment, resources and sustainable development) for his availability and for giving me the precious opportunity of visiting the historical “Accademia Liuteria Piemontese – San Filippo”, directed by master lute-maker Enzo Cena in Turin.

Thanks to professors Marco Masoero and Louena Shtrepi of DENERG (Department of Energy at Polito) for their support, in particular to Prof. Shtrepi for her lecture on general acoustic.

Prof. Carlo Rosso (DIMEAS) for his support on the evaluation of the loads, tensions and deformations on the frog’s plates.

Francesco Stoppani, Application Sales Engineer at Festo, for his consultancy in the design of the bowing machine.

Thanks to the manufacturing company OCMA, of Gianluca Esposito, in Turin, for the realization of the bow’s frog device.

Last, but not least, my family, for their unconditional love and support during all these years.

1. Introduction: the bowed string state of the art

Since the end of the 19th century many studies were conducted in order to understand the working principle of the violin, and similar instruments. In this direction, the first remarkable results were obtained by Hermann von Helmholtz; in 1863 he published *Die Lehre von den Tonempfindungen als physiologische Grundlage für die Theorie der Musik* (translated as *On the sensations of tone*) which represents a milestone for acoustics, after his studies on the interaction between the sound wave and the human perception of the sound itself [1]. In addition, he theorised the so-called stick-slip motion, which will be examined in the next chapter; basically, it consists in a continuous transition of the string between a sticking and sliding friction condition in relation to the bow. Since then, the understanding of this phenomenon has gradually increased, and today the motion of the bowed string is considered as one of the few examples of vibration triggered by friction which could claim to be reasonably well understood.

Later on, Chandrasekhara Venkata Raman published in 1918 a work where he defined some models he obtained, through several assumptions of an idealized string, that would be able to describe the whole dynamics of the bowed string vibration (supported by experimental results) and that could be solved simply by hand [9], way longer the computer age; his contribution to the study of this phenomenon are nowadays considered as very important and a valuable extension of the Helmholtz's ones.

After more than a century from the first observations of Helmholtz, thanks to the increasing improving of computer simulations which allowed for more realistic models of the bow-string dynamics, John C. Schelleng in 1973 formalized the limits of some bowing parameters (like force to be applied on the string with the bow and bow-bridge distance) that would allow the player to obtain a pleasant sound and summarised all this information into the so called Schelleng diagram [3].

Later refinements on a more detailed level, but still very relevant from the string player's point of view, included more sophisticated friction models and influence of other parameters on the quality of the sound, like the bow acceleration and the bow velocity analysed respectively by Guettler in 2002 [4] and Schoonderwaldt in 2009 [2], that allowed an improvement of the Schelleng diagram, in a direction much closer to the real case.

1.1 Helmholtz theory and concept of ideal string

As mentioned in the introduction, the regular vibration of a bowed string was analysed by Helmholtz in 1863, using an adapted version of a vibration microscope. His observations allowed him to derive a kinematic description of the motion of the whole string. Helmholtz discovered that the motion of the bowed string could be described by a travelling corner, as represented in Figure 1.1.1, travelling back and forth on the string along a parabola-shaped path (dashed line). The bow is applied along the direction x_B , with constant velocity v_B , and it is closer to the bridge rather than the nut (for the geometry and nomenclature of the violin, refer to Figure 1.4.1).

The travelling corner is assumed as perfectly sharp (on an idealized, perfectly flexible string). At any position along the string, the displacement, as a function of time, is described by a triangular wave, whose slope depends on the point of observation. Correspondingly, the string speed is characterized by two alternating values: v_+ along the direction of the bowing movement and v_- on the opposite direction, respectively.

The period of vibration T is determined by the time it takes the corner to make a complete round trip. At the moments t_3 and t_4 the string is sticking to the bow and, for case (b) represented in Figure 1.1.1 where the observation point is placed directly under the bow, its velocity corresponds

to the velocity v_B of the bow itself, while at the instants t_1 and t_2 the string slips from the bow; it could be noticed how the sticking phase lasts longer but at a lower absolute velocity, while the slipping phase occurs in a shorter time with a higher absolute velocity v_S of the string, in the opposite direction. In case (c), the observation point corresponds to the middle of the string x_M . As the string follows the motion of the bow during sticking, the amplitude of the string vibrations is determined mainly by the combination of bow velocity and the relative bow-bridge distance: the string vibrations amplitude value is proportional to the bow velocity v_B , and inversely proportional to the relative bow-bridge distance β (where β is defined as the bow-bridge distance x_B divided by the total length of the string L).

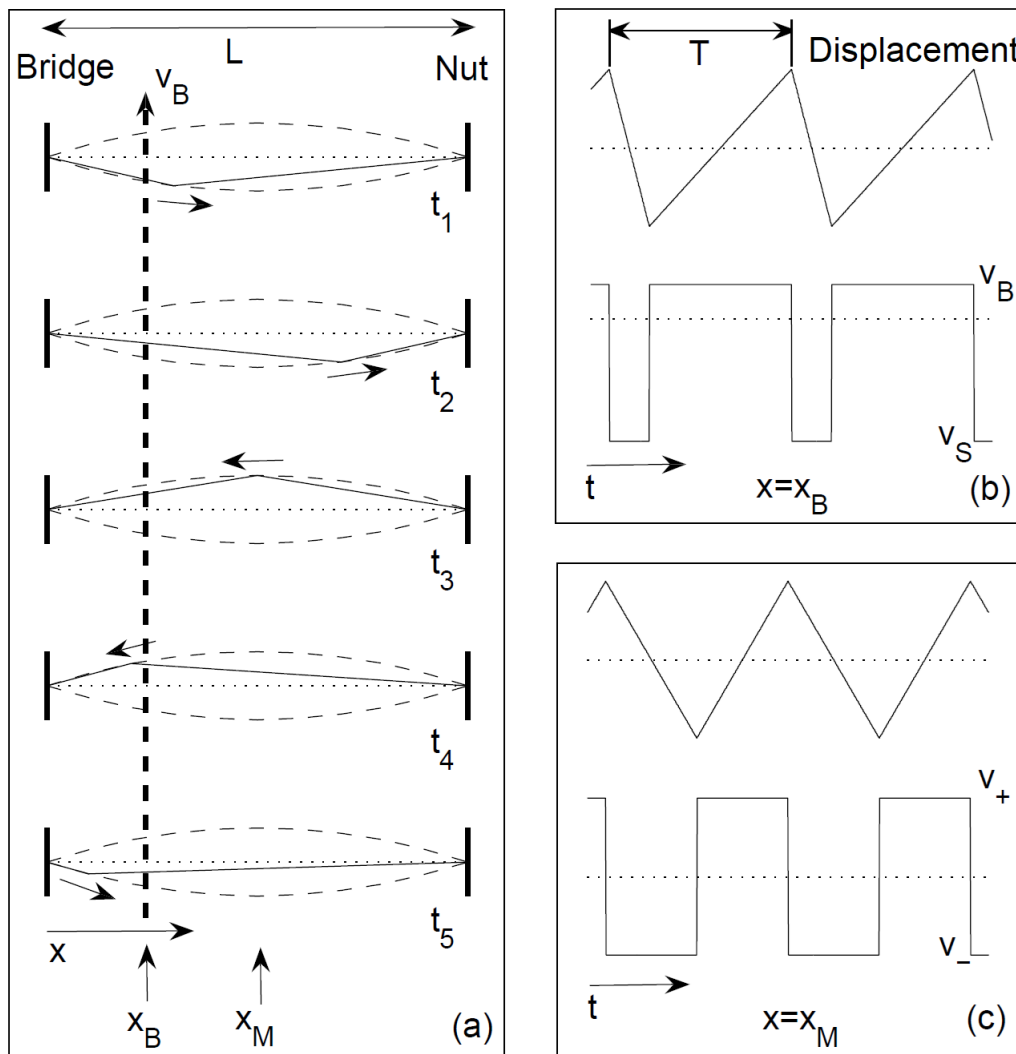


Figure 1.1.1 – Description of Helmholtz motion.

1.2 Bow force limits in a real case: the Schelleng diagram

As seen above, the idealized Helmholtz motion is characterized by a perfectly sharp corner that travels, during one period, between the bridge and the nut along an elliptical cycle. This description of the ideal bowed string corresponds to a free oscillation without losses, which could as well take place in absence of the bow. The excitation force contribution coming from the bow (the force with which the bow is pressed against the string) was not yet considered in the ideal model.

For a real string, energy losses and stiffness matter. In this case an excitation received by the bow is required to keep the string vibrating. This excitation (the bow force), for the maintenance of regular Helmholtz motion, characterized by a single slip and stick phase per fundamental period T , must be contained within a defined range, which involves two requirements: during the sticking phase the bow force must be high enough in order to avoid a premature slipping under influence of variations in frictional force (but within a certain upper limit), and during the slipping phase it must be low enough so that the traveling corner, when it arrives at the bow, can trigger the release of the string. Raman, in another classic of musical acoustics, extended Helmholtz's work and clarified the aspects introduced above and many other regarding the bowed string, including a calculation of frictional driving force and the manner in which velocity and position of the bow as well as the frequencies of resonance of the instrument affect the minimum bow pressure.

As already mentioned in the introduction, in 1973 Schelleng, based on the conclusions coming from the Raman's string model, obtained the equations for the minimum and maximum bow forces and in this way formalized the limits of the playable region. He introduced a graphical representation of his results, choosing as bowing parameters the relative bow force versus bow-bridge distance (both on logarithmic scale) at a fixed bow velocity, as shown in Figure 1.2.1.

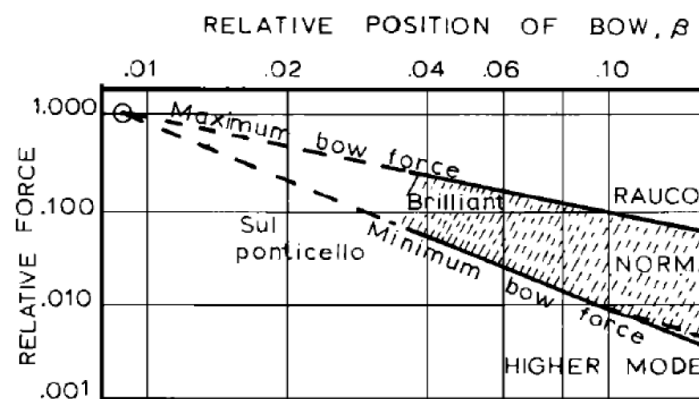


Figure 1.2.1 – Schelleng diagram.

The maximum and minimum bow-force limits are represented as straight lines with slopes of -1 and -2, respectively. The friction coefficient δ is assumed as constant.

As indicated, the string motion beyond the upper bow-force limit is characterized by raucous, aperiodic motion, corresponding to a scratchy sound. Below the lower bow-force limit the string motion is mainly characterized by multiple slipping, with two or more slipping phases per fundamental period (which is not acceptable), thus corresponding to a “whistling” sound.

Moreover, it could be appreciated how the shorter is the relative bow-bridge distance, the narrower is the allowed range of bow force.

1.3 Influence of the bow acceleration: the “attack”

In the above description of the bowed string, only steady-state vibrations have been considered. Actually, a proper start of the tone, which corresponds to a quick development of the Helmholtz motion, is as important in performance evaluation as the steady state. The conditions for the start of the tone (the so-called “attack”) have been formalized by Guettler, in 2002, and are graphically represented in Figure 1.3.1.

The diagrams show different triangle-shaped playable areas as a function of bow acceleration, bow force and relative bow-bridge distance β ; in particular, while β is kept fixed, the other two

parameters are varied. Moreover, there is a direct comparison between predicted behaviour and simulated results coming from computer simulations.

The numbers on top, spanning from 0 (in white) to 5+ (in black), represent the required periods of oscillation before the development of the Helmholtz stick-slip motion occurs (ideal condition). Therefore, the white area indicates a “perfect” attack, characterized by a quick development of the Helmholtz motion from the first period. With too high values of bow force and too low bow acceleration the attack is characterized by prolonged periods (“choked/creaky” sound). On the other hand, when the bow force is too low and acceleration too high, multiple slipping (“loose/slipping” sound) occurs. Also, for smaller values of β the triangle for the perfect attack becomes narrower, which could result in a higher effort for the player.

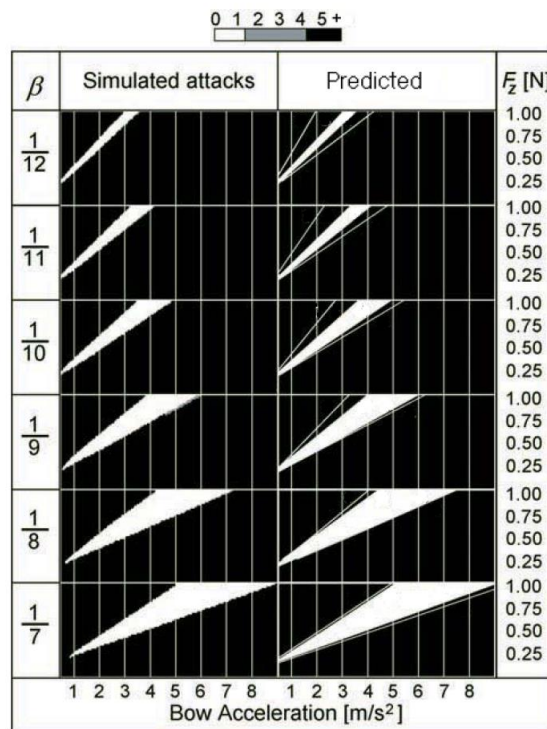


Figure 1.3.1 – Guettler diagrams.

1.4 Acceptable bowing parameters values

To summarise all the most interesting (for the sake of this work of thesis) theories discussed so far, the main bowing parameters for the control of sound that can be useful for the player are basically three, with the acceptable ranges of values indicated in the brackets (specific adopted nomenclature in Figure 1.4.1):

- Bow velocity (5–100 cm/s): the velocity of the bow as imposed by the player’s hand at the frog. The local velocity at the contact point with the string is not exactly the same due to small bending in the bow hair and vibrations of the stick. The bow velocity determines the amplitude of oscillation of the string, together with the bow-bridge distance;
- Bow-bridge distance (5–60 mm): the distance along the string between the contact point with the bow and the bridge;
- Bow force (0.1–2 N): the force with which the bow hair is pressed against the string at the contact point. The force direction is normal to the plane occupied by the main body of the violin. The bow force determines the timbre (“brightness”) of the tone. As explained in the previous

chapters, to obtain tones of regular quality (Helmholtz motion) the bow force needs to stay within a certain range. The upper and lower limits for this range of bow force both increase with increasing bow velocity and decreasing bow-bridge distance.

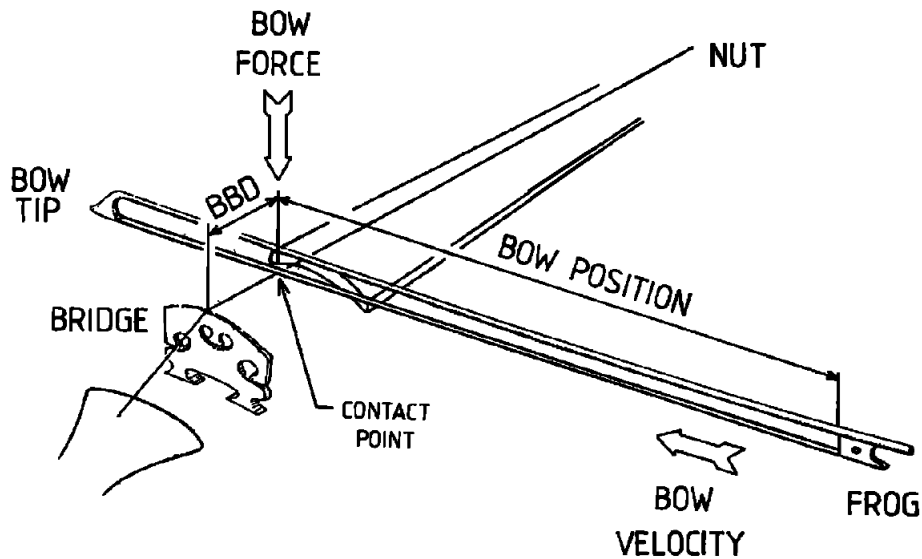


Figure 1.4.1 – Violin bowing parameters scheme.

1.5 Influence of the bow velocity: uncertainty on Schelleng lower bow force limit

Before proceeding on the second part of this work of thesis, with the analysis of the history of the bowing machines and the tools for data acquisition taken into consideration, it would be relevant to briefly introduce the latest studies on the bowed string of musical instruments, developed by Schoonderwaldt in 2009, which have underlined a closer relation between the bow velocity and the playable region of the violin through some measurements that questioned also the reliability of the lower limit of bow force defined in the past by Schelleng and seen in chapter 1.2.

By adopting a computer-controlled bowing machine, which allowed a perfect repeatability of the bowing gesture and a systematic and accurate control of the main bowing parameters, Schoonderwaldt analysed many combinations between these parameters, on a rigid monochord of the same dimensions as a standard violin. The monochord was chosen in order to focus on the string conditions, thus avoiding the influence of the vibrational modes of the violin.

What he found out are a set of different experimental Schelleng diagrams, as shown in Figure 1.5.1, obtained with four different bow velocities (5, 10, 15 and 20 cm/s). The Helmholtz motion is respected inside the light green squares region, while multiple slipping and raucous motions were witnessed respectively in the blue pluses and in the red x-marks areas.

By comparing the four different graphs, it can be appreciated a slight discrepancy in the upper limit between the prediction coming from the Schelleng diagram theory (solid black line) and the experimental results obtained by Schoonderwaldt (black dashed line), which is more evident at lower bow velocities, in panels (a) and (b), where the new limits appear to be less steeper than the theoretical ones.

Moreover, the upper bow force limit was confirmed to be proportional with bow velocity (the threshold is shifting higher linearly with bow velocity); at the same time a higher bow velocity increases the playable region. On the other side, it is interesting to notice how the lower force limit segment is mostly independent from velocity. This last point is the most controversial one that started the discussion about the validity of the lower force limit on the Schelleng diagram, since

what was expected from the Schelleng's equations was the complete opposite. By reassuming, what Schoonderwaldt and his team noticed is that the assumptions on which Schelleng based his evaluations were coming from the Raman simplified string model in which all the energy losses, included internal damping of the string and the damping caused by the finger used by the player to stop the string were not considered. In this kind of application, damping is instead a very important factor and should be taken into account in order to obtain an evaluation which is much closer to reality. These assumptions generated the discrepancy between the Schelleng diagrams and the Schoonderwaldt ones.

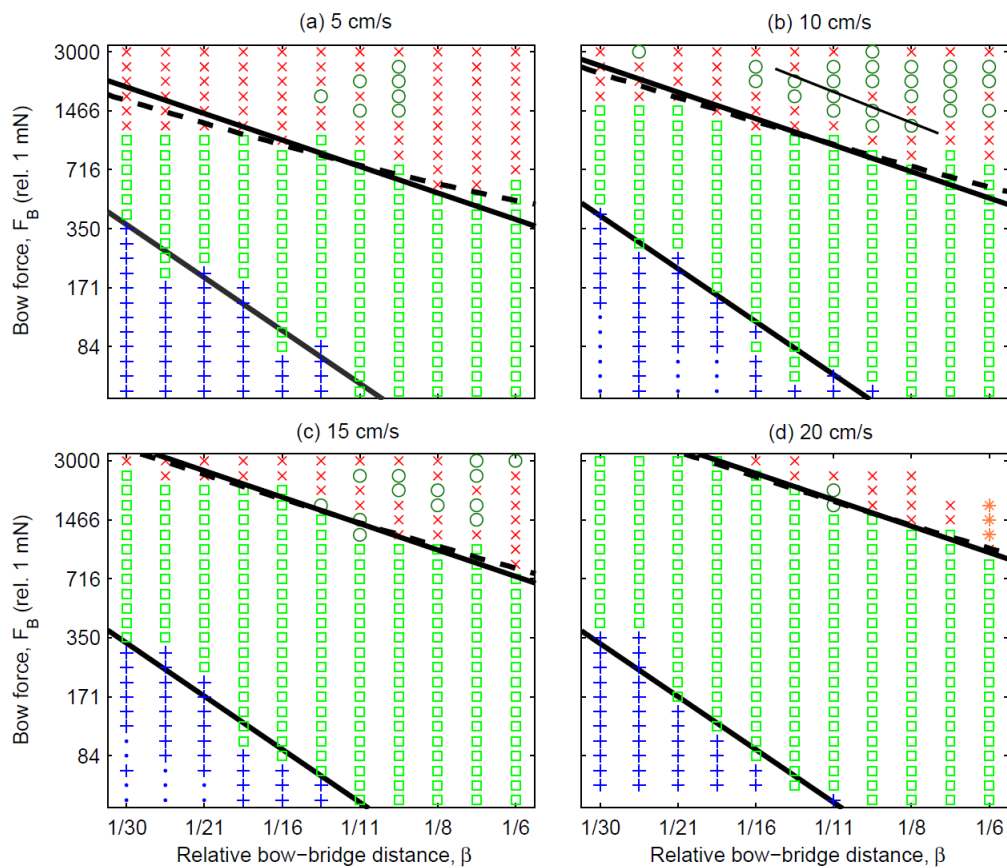


Figure 1.5.1 – Experimental Schelleng diagrams in 4 different bow velocity configurations.

Anyway, the reader shall keep in mind that the sake of this work of thesis is not to verify the validity of one theory or another; this whole excursus was just presented in order to define the range into which the requirements for the design of the test rig for the violin performance evaluation shall sit, as a sort of guideline. The Schoonderwaldt theory introduced in this last chapter could surely represent an interesting starting point for further research, in case of future developments on the subject.

2. Test rig design introduction

After having defined which parameters shall the bowing of the string respect, it is fundamental to define how to apply these concepts to the bowing gesture itself. It is relevant to understand that a violinist, even the most talented one, would never be able to repeat the same gesture exactly in the same perfect way over a certain period of time, even if the gestures will be for sure very similar one to each other. So, one important characteristic that the bowing gesture must respect is the repeatability; one way to realize this is to adopt a bowing machine.

In the next chapters, it will be presented an excursus of the most interesting bowing machines (both mechanical and controlled) that have influenced this work of thesis, with a focus on the key role of the bow frog in the transmission of the excitation to the string. After that, in order to respect the bowing parameters proposed in the first chapter, two schemes of static loading conditions of the string will be presented, first by applying a constant force at the tip of the bow by use of a weight and second by applying a constant torque at the bow frog, and in this scheme the reactions on the frog and the string themselves will be computed.

2.1 Bowing machines state of the art

In the past, researchers have tried several methods to bow violins in a mechanical manner (Saunders, 1937 [11]; Bradley, 1970 [13]; Coates, Higgs, Parsons, & Townsend, 1975 [14]; Barnes, et al., 1983 [12]). Since they primarily were interested only in the properties of the violin, they usually did not use a real bow for the excitation of the string. Instead, the bow hair was mounted on some simpler moving or rotating device in order to make the instrument sound, as schematized in Figure 2.1.1. In some cases, the bow hair were replaced with rosin, to simulate the same behaviour.

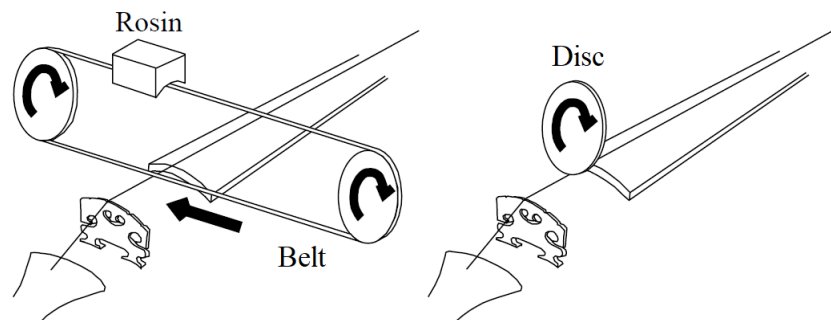


Figure 2.1.1 – Early bowing machines schemes.

One popular way of bowing machine has been to mount a loop of bow hair between two wheels as shown in Figure 2.1.2. Another solution, adopted by Saunders in 1937, has been to use rotating discs of celluloid which were treated with rosin on surface to simulate the bow hair, as in Figure 2.1.3. A few bowing machines used a real bow to excite the string like the one in Figure 2.1.4 (Raman, 1920 [16]; Lawergren, 1980 [15]). The peculiarity in the system used by Raman is that the bow was fixed, and the violin is moved by a mechanism, while the ones seen previously were keeping the violin fixed.

All these old bowing machines had a limit that is they could only be used for taking measurements under steady-state conditions, often by measuring the radiated sound and obtain the response curves.

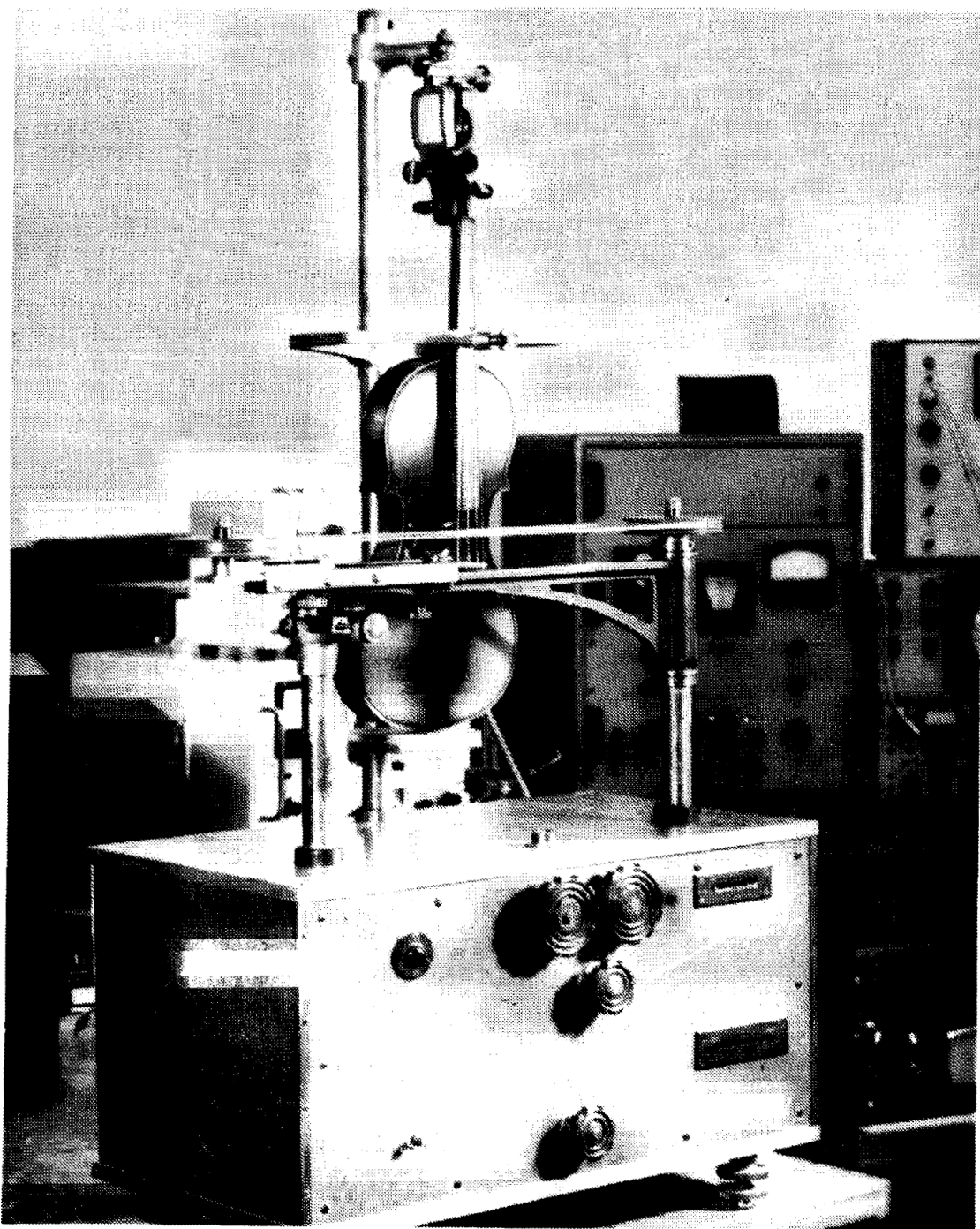


Figure 2.1.2 – Early bowing machine using a rotating loop of bow hair to excite the string.

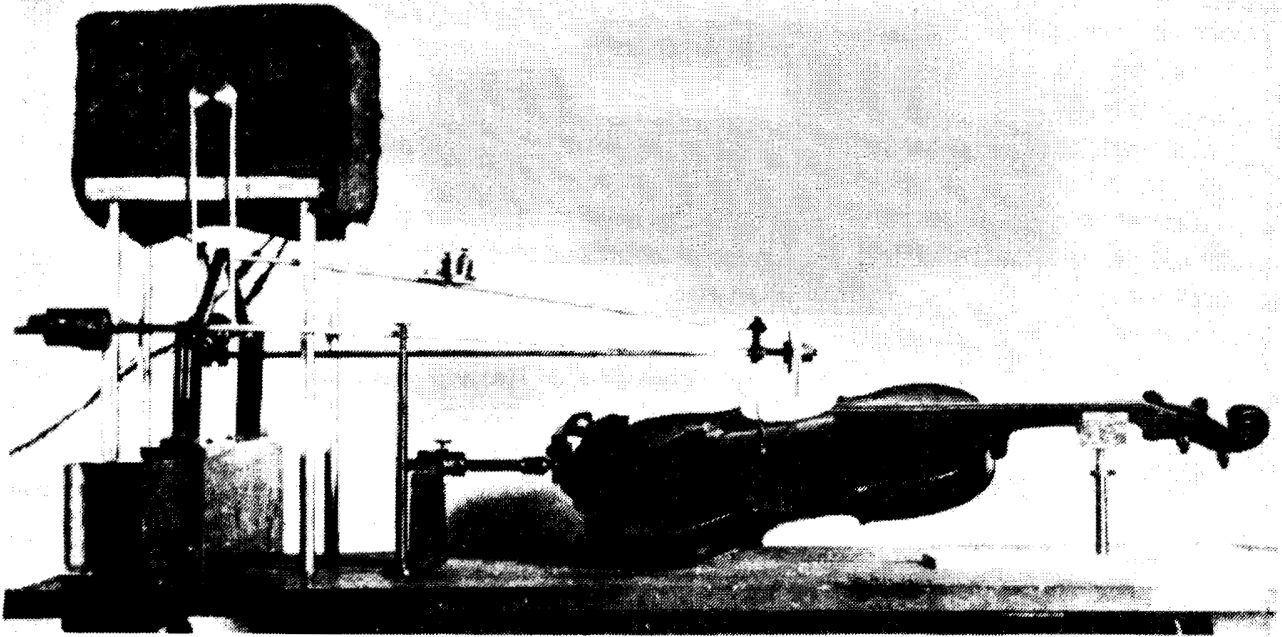


Figure 2.1.3 – A bowing machine using a rotating disc to excite the string (Saunders, 1937).

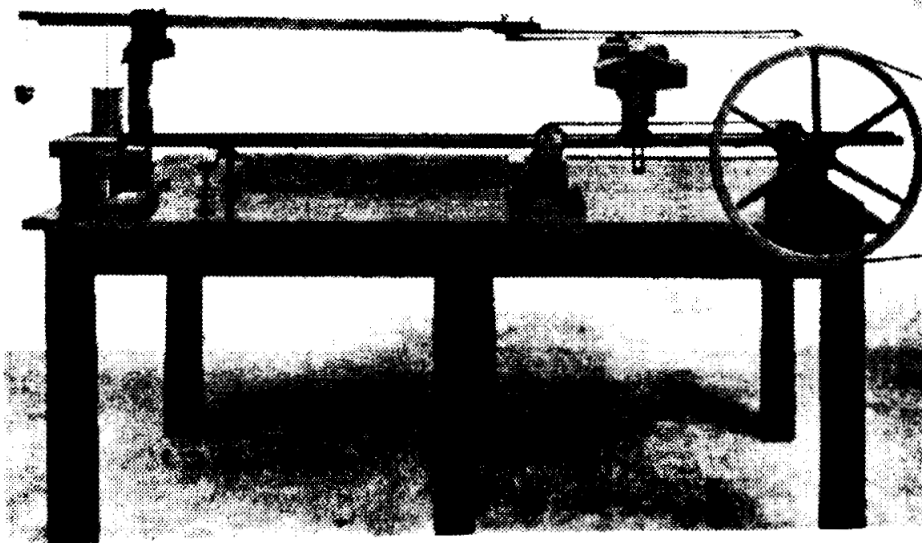


Figure 2.1.4 – A bowing machine using a normal bow to excite the string (Raman, 1920).

Later on, in 1992, Cronhjort made a big step forward in the development of the bowing machines with MUMS [6] (which stands for MUsicerande Maskin för Stråkar, literally translated as “Machine to make music for bows”), by adding the computer controls to the mechanics, as schematized in Figure 2.1.5. MUMS was composed of two parts: a main part made of a printwheel coming from a printer which contains the mechanical support of the bow and the motors for bow motion and force, interfaced with a computer which controls the motion by software servos, throughout a PID-algorithm for the position. The violin is fixed, at the side of the machine, while the bow is clamped to a carriage (formerly carrying the printwheel) which can move along a rail supported by linear roller bearings. The carriage is pulled by the original DC-motor through a belt. The maximum stroke is about 330 mm.

The bow position and velocity are controlled by a software servo, with the position feedback read optically on the shaft of the carriage motor. The maximum reached velocity is approximately 1 m/s.

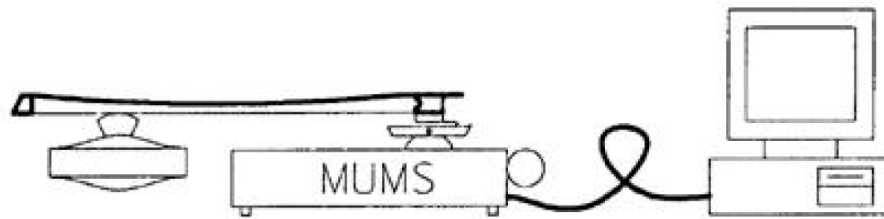


Figure 2.1.5 – MUMS overview (Cronhjort, 1992).

The bow force is controlled by applying a torque to the frog (handle) of the bow. This is done by slightly rotate the carriage by means of an electrical motor. The bow is not clamped directly to the carriage but to a some kind of flexible cantilever, which bends as a torque is applied. What is mounted directly on the carriage is the motor that controls the torque (as said, formerly rotating the printwheel). The torque is controlled by a second software servo, which computes the actual bow force at the point of contact with the string, knowing the position of the bow (and violin) from the PID algorithm.

The feedback to the servo is obtained from strain gauges, mounted on the cantilever, measuring the bending, and thus indirectly the torque. The bow frog mounting detail just explained is shown in Figure 2.1.6. The maximum torque applied was approximately 0.6 Nm, corresponding to a maximum bow force at the tip of almost 1 N (which is lower than the upper limit value of 2 N imposed in chapter 1.4).

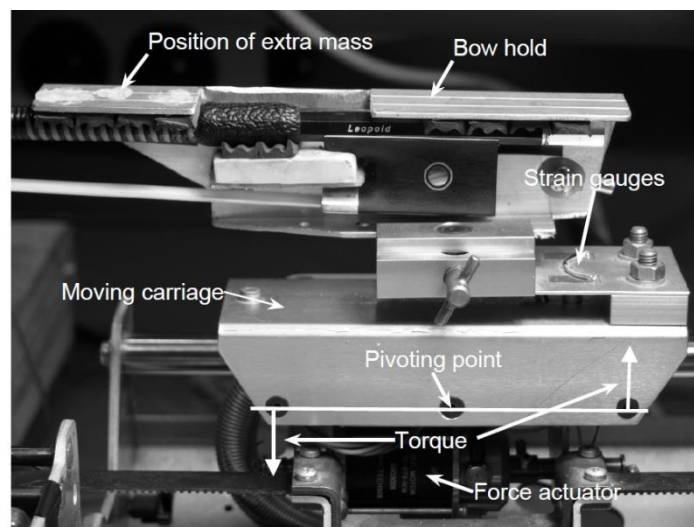


Figure 2.1.6 – Bow frog mounting scheme detail in MUMS (Cronhjort, 1992).

Another interesting solution comes from the experience of Galluzzo in 2003 [10]. He connected a shaker to the bow in order to excite the string with some impulses of 1 second duration; the “bow” consisted of a Perspex rod (plastic material) mounted in a cantilever arrangement on a 2 mm thick leaf spring made of mild steel, pressed against the string by the shaker. The whole system is pulled back and forth using a linear motor, making the instrument play. In this case a leaf spring rather than a pin joint or hinge was adopted because this solution could be designed to be flexible enough not to resist the action of the shaker (ideally it would mimic a perfect hinge when the shaker pushes the bow into the string). To provide the linear movement of the Perspex rod, necessary to play the violin, the rod, the leaf spring and the shaker are all mounted onto a linear induction motor.

The scheme of the mechanical design (not to scale) is depicted in Figure 2.1.7. It can be also appreciated the position of the strain gauges, on the built-up bow frog, for the indirect measure of

bow/string contact force. In Figure 2.1.8 it is represented a picture of the so far described bowing machine adopted by Galluzzo in which the scale of the whole system can be appreciated.

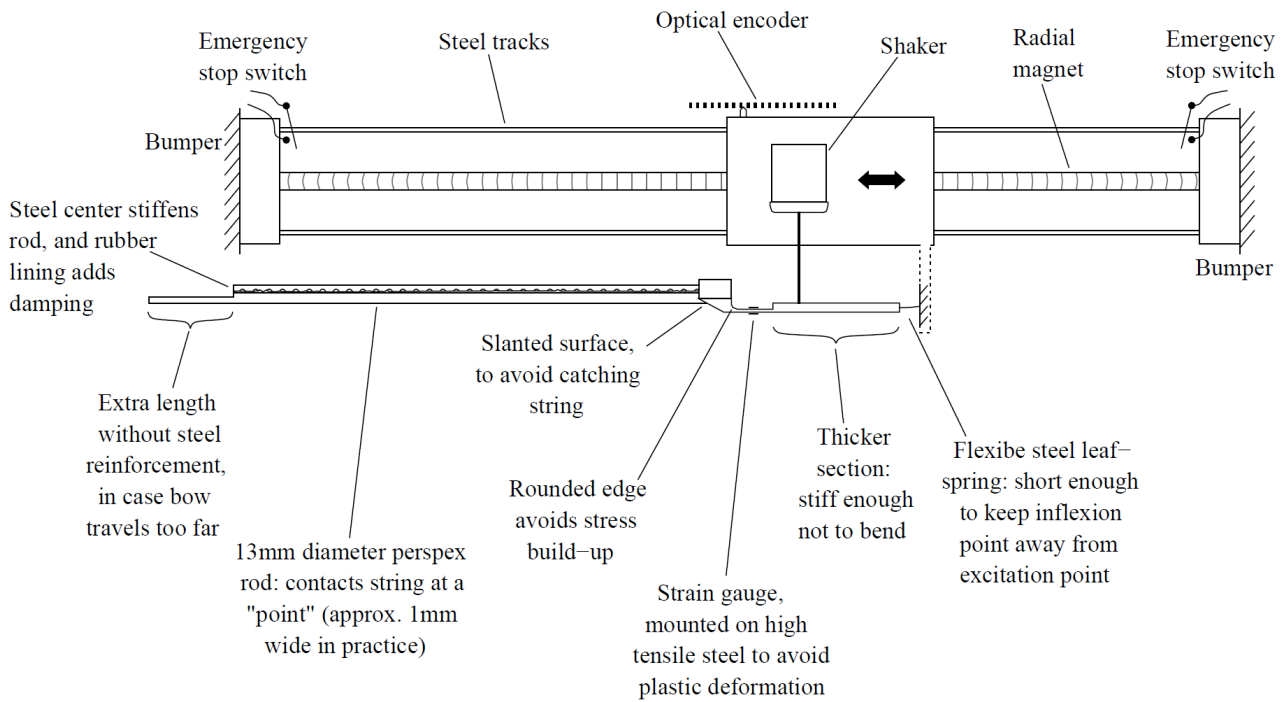


Figure 2.1.7 – Bowing machine drawing (not to scale) scheme (Galluzzo, 2003).

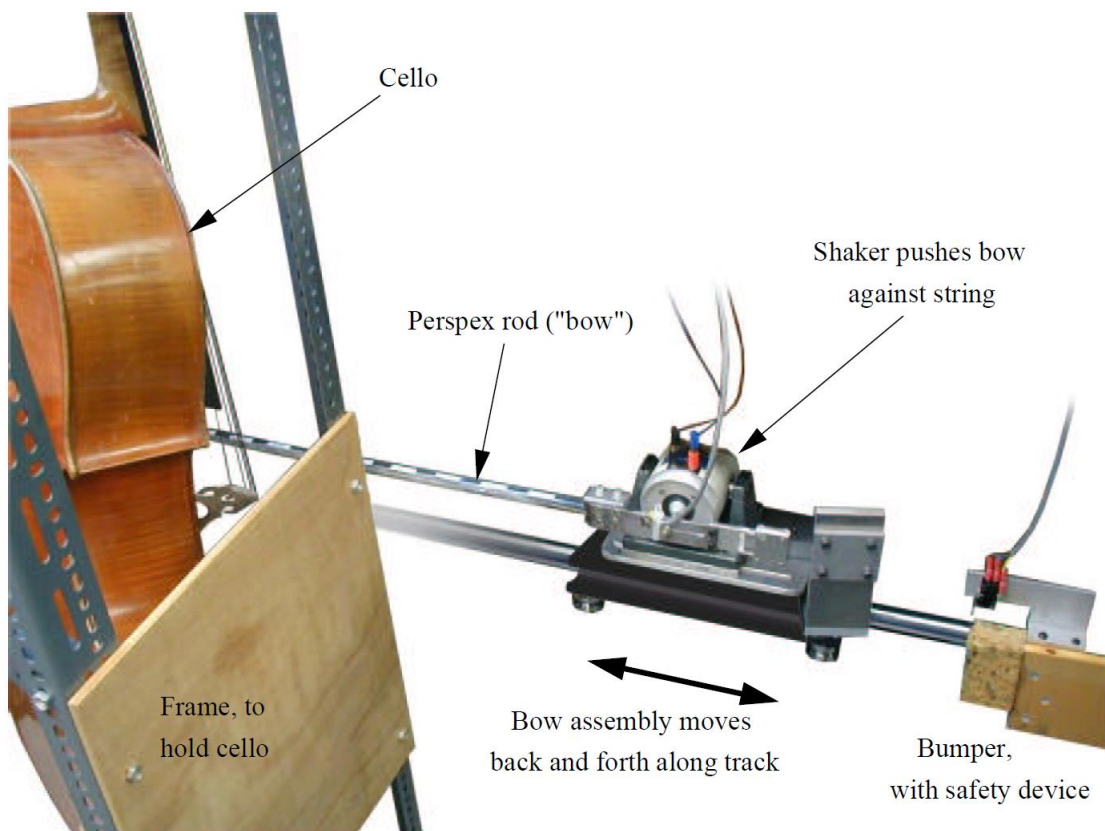


Figure 2.1.8 – Bowing machine picture (Galluzzo, 2003).

How it can be noticed from the last two solutions presented, all the actions that excite the string pass through the frog, which in this case plays a fundamental role in the design of a proper bowing machine. That is why, the next step in the development of the test rig, is to find out what kind of reactions are acting on the frog and the string, for two different schemes of static loading. The bow will be hypothesized as connected to a linear actuator which moves in the horizontal plane.

2.2 String-Bow static loading condition

As previously seen from the evolution of the bowing machine technology, there are basically two different methods for exciting the bow with the string: either by literally “pushing” the bow against the string through a normal force (as in the case of Galluzzo), or by applying a torque to the frog (solution adopted by Cronhjort). So, another necessary step in the design of the test rig is the analysis of these two solutions, from a static loading condition point of view.

Basically, with the same scheme already seen in Figure 1.4.1, the bow itself was considered as a cantilever beam, hinged in the point corresponding to the frog (B), and the contact point, between the string (its axis normal with the plane containing the bow axis) and the bow hair, considered as a roller (C), which can move freely along the direction of the bow, thus producing a vertical reaction with it, as seen in overview in Figure 2.2.1.

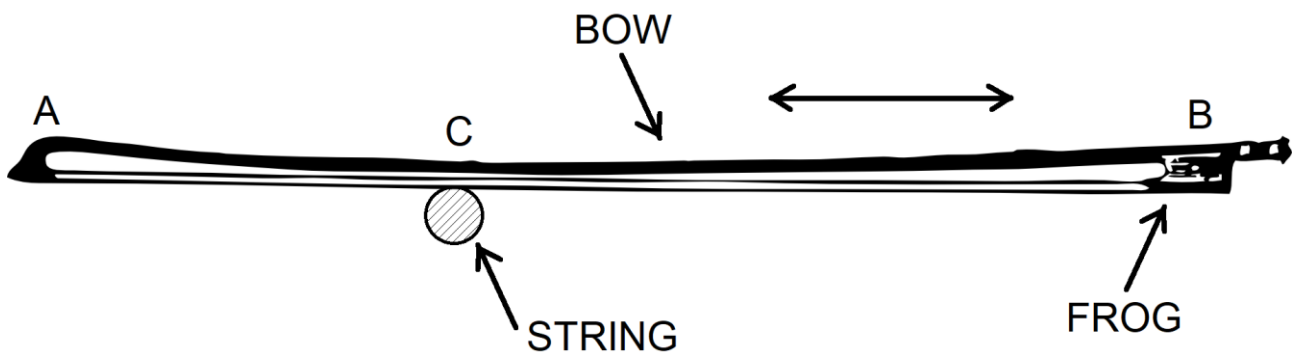


Figure 2.2.1 – Plane containing bow and string

The main target was to evaluate how the reaction acting on the string changes along the bow’s length, while the bow excites the string in two different loading conditions. The total bow length considered is L_b equal to 65 cm and its weight m_b equal to 60 g.

2.2.1 Constant vertical load

The first analysed static loading condition considers a very small mass m (respectively of 100 g, 50 g and 20 g) connected at the tip of the bow (Figure 2.2.1.1), which keeps the bow pushed against the string. Point B would represent the ideal connection point between the support on a linear actuator that can move on the horizontal plane (1 degree of freedom) and the bow’s frog. Point G corresponds to the bow’s centre of gravity, where the whole mass of the bow is concentrated. Point C is the contact point between the bow and the string, and it is the only one whose distance from the bow’s ends can vary (length L), and point A is the bow’s tip.

The reactions on the free body diagram of the bow are schematised in Figure 2.2.1.2. In order to find the reactions, the following two equations for the equilibrium must be solved:

$$mg + m_b g = R_B + R_C$$

which represents the vertical reaction equilibrium, and

$$R_C L = mgL_b + m_b g \frac{L_b}{2}$$

which represents the moment equilibrium around point B.

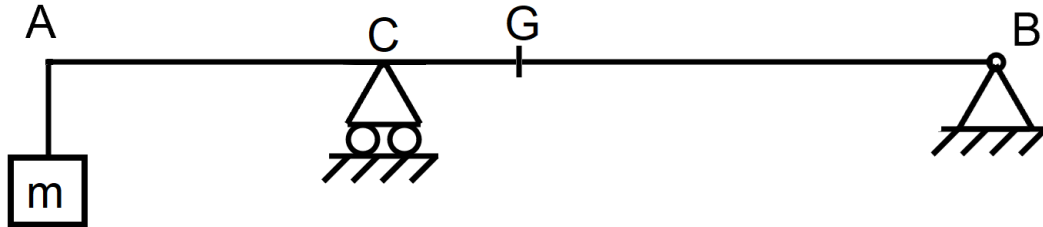


Figure 2.2.1.1 – Constant vertical load scheme.

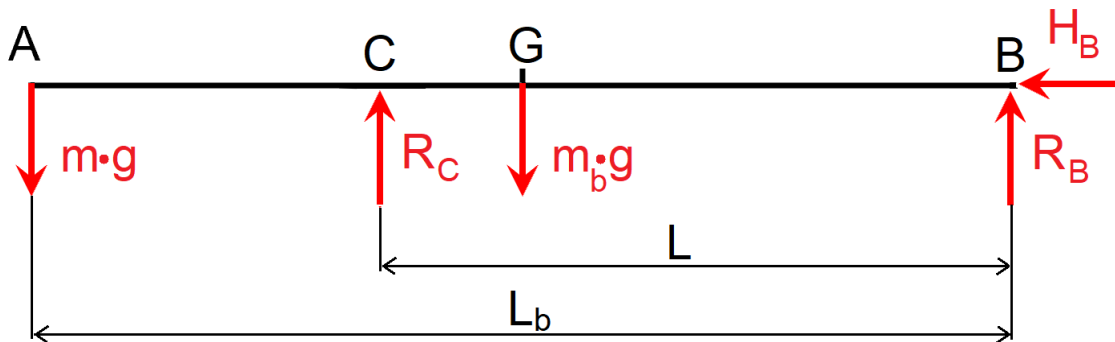


Figure 2.2.1.2 – Constant vertical load scheme reactions.

The formula for the evaluation of the reaction in C (on the string), as a function of the distance between the contact point and the frog is obtained from the second equilibrium equation:

$$R_C(L) = \frac{mgL_b + m_b g \frac{L_b}{2}}{L}$$

for $0 \leq L \leq L_b$.

In the same way, the vertical reaction on the frog is evaluated through the first equilibrium equation:

$$R_B = mg + m_b g - R_C$$

By adopting different values for the additional mass, the following results in Figure 2.3.1.3 have been obtained. Some considerations can be done by observing the two graphs: by using relatively small additional masses at the tip of the bow, it is easy to get close to the upper threshold of bow force equal to 2 N, which was defined in chapter 1.4; in some cases, by getting closer and closer to the frog (point of contact which tends to 0 m) and in the same time increasing the additional mass, this threshold is even passed. This is caused by the fact that the contact point distance is at the denominator in the equation of the reaction of the string in C, which tends to infinite for L tending

to zero. The reaction on the frog has mostly negative sign, which means that its direction in the reaction scheme in Figure 2.2.1.2 shall be changed on the opposite way (pointing downward). All things considered, from the analysis of the static loading of the bow/string interaction, when dealing with a bow mounted on a linear actuator (of a test rig) it would be important not to operate in the region closest to the frog (between 10 and 20 cm from it); by doing so, for an additional mass smaller than 50 g, the reaction on the string is consistent.

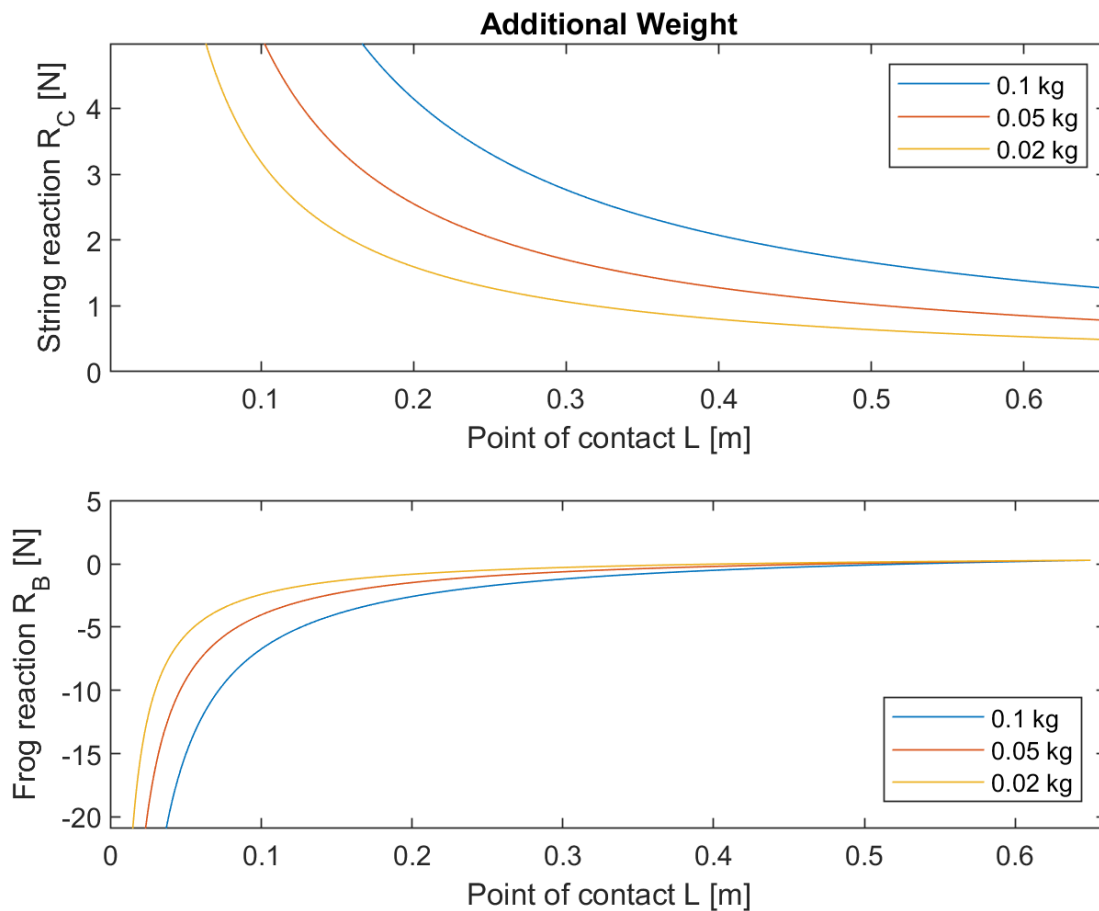


Figure 2.2.1.3 – String and frog reactions behaviour with additional mass loading conditions.

2.2.2 Constant external torque

The second analysed static loading condition replaces the additional mass at the tip of the bow with an external torque applied on the frog (Figure 2.2.2.1.), which keeps the whole bow pressed against the string.

The reactions on the bow are schematised in Figure 2.2.2.2.

The equilibrium equations to be solved in this case are:

$$m_b g = R_B + R_C$$

$$R_C L = m_b g \frac{L_b}{2} + C_{\text{ext}}$$

which lead to the following function for the vertical string reaction in B:

$$R_c(L) = \frac{m_b g \frac{L_b}{2} + C_{ext}}{L}$$

for $0 \leq L \leq L_b$. For the reaction on the frog the equation to be solved is:

$$R_B = m_b g - R_C$$

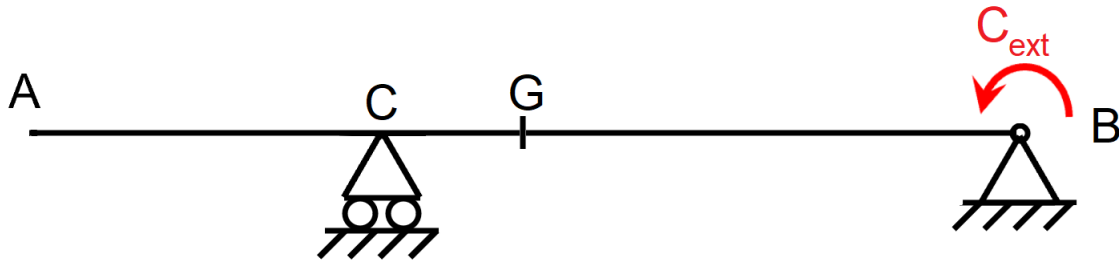


Figure 2.2.2.1 – Constant external torque loading scheme.

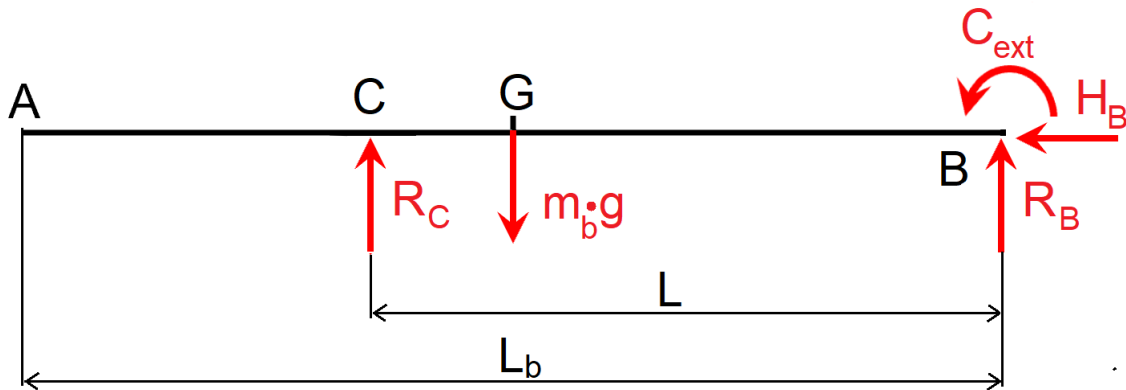


Figure 2.2.2.2 – Constant external torque static loading scheme reactions.

By adopting different values for the external torque, the following results in Figure 2.2.2.3 have been obtained.

The results are very similar to the ones observed in the case of additional constant mass. Even for a relatively small amount of external torque of 1 Nm, it is easy to pass the threshold of 2 N for the reaction on the string; for smallest values of torque, it is important again to operate far from the frog area. For what concern the reaction on the bow instead, here seems to be more dependant from the value of the external torque applied than the previous case of additional mass, as the three curves are further from each other. Again, as the contact point distance is at the denominator in the equation of the string reaction, it causes the reaction to tend to infinite for L tending to zero. In the same way, as already seen, the direction of the vertical reaction on the frog R_B must be changed in the opposite way, on the initial free body diagram in Figure 2.2.2.2, as it is always negative in the graph in Figure 2.2.2.3.

In conclusion, since the observed behaviour of the string reaction is quite the same with both static loading conditions, the first one with the additional mass at the tip of the bow was considered in the

next chapter, for the building solution of the test rig proposed by Festo, for a matter of constructive simplicity, rather than applying a constant external torque on the frog.

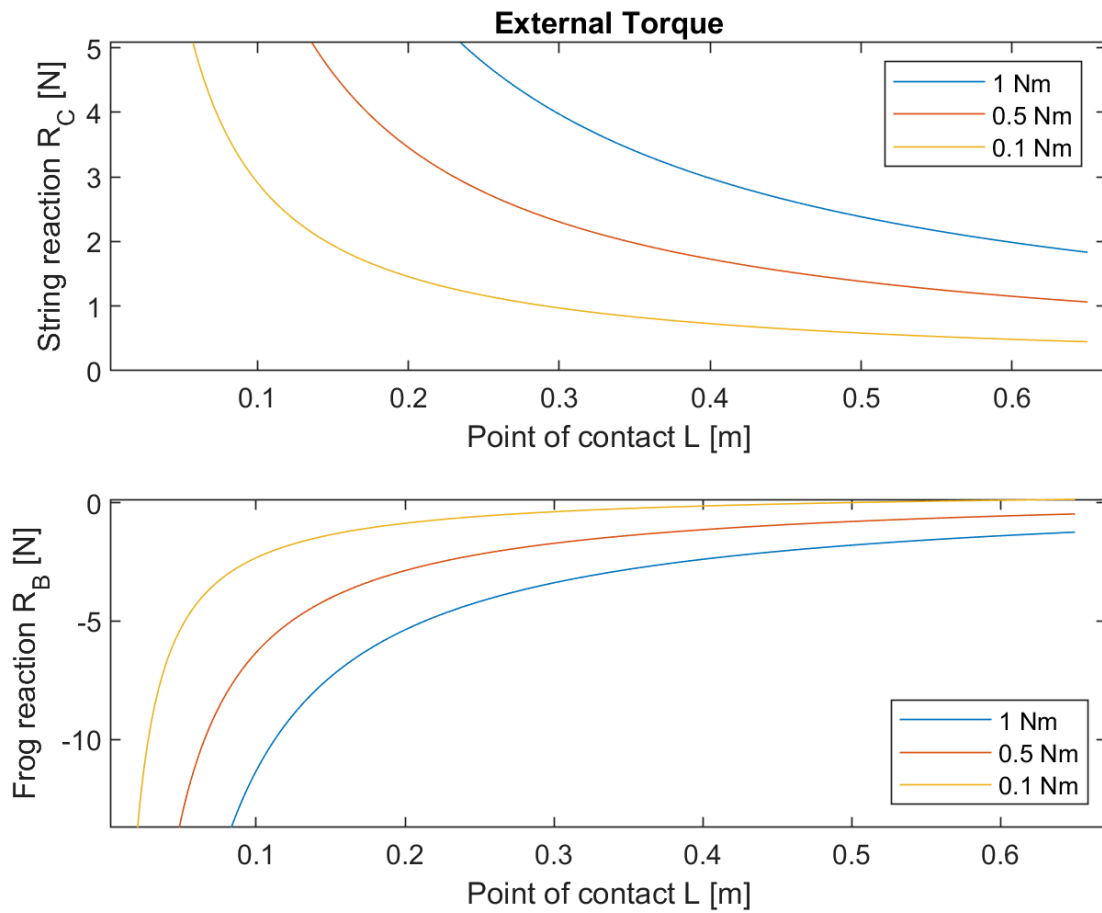


Figure 2.2.2.3 – String and frog reaction behaviours with external torque loading conditions.

3. Test rig realization

Now that the theory behind the bowed string (in chapter 1) and the main influencing bowing machines ideas (in chapter 2) have been introduced, it is time to deal with the main part of this work of thesis, which is the realization of the bowing machine itself (the test rig) for the evaluation of the acoustic performance of a violin.

In particular two solutions will be proposed; the first one has been discussed with Festo (one of the leading companies in the pneumatic and electrical automation sector) and involves the building of a whole bowing machine, consisting of a linear actuator, an electrical engine and a controller. The solution itself will be analysed from both a technical and an economic aspect.

In the second solution, it will be showed a modified concept of the bow, with a focus on a different design of the frog (the bow handle), to be implemented with sensors (strain gauges), in order to obtain directly the measurements of bow force. This second solution has been physically built and could be adopted with both a bowing machine or without it; in the second case the string must be bowed directly by the player, which is definitely cheaper than the realization of the whole bowing machine, but unfortunately it would make fall the advantage of the repeatability of the bowing gesture.

3.1 Bowing linear machine solution proposed by Festo

From the analysis of the bowing machines done in chapter 2, the most suitable configuration scheme chosen is the one depicted in Figure 3.1.1, which is comparable with the one obtained by Cronhjort with MUMS (Figure 2.1.5). The whole system is to be intended as mounted horizontally, with the violin's side facing the actuator.

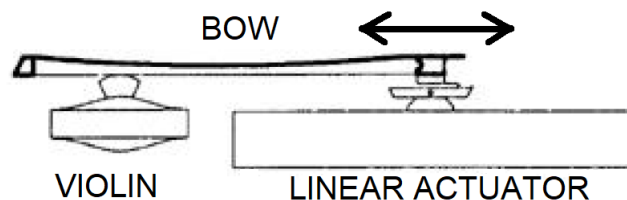


Figure 3.1.1 – Bowing machine configuration scheme.

The realization of the complete bowing machine has been discussed by the German company Festo, and in particular with Francesco Stoppani, the Application Sales Engineer, who proposed a positioning-kind solution; after having defined with him the operating boundary conditions (presented in the first chapter) and run a simulation with an hypothetical load, through the software Positioning Drives (V2.3.25) supplied by Festo, the main components (with the relative catalogue nomenclature), are summarized in Figure 3.1.2.

As can be noticed by the picture below, basically, the bowing machine is composed of three main parts:

- The structure is constituted by a gantry linear drive axis (ELGC) made of a toothed belt (TB) guided by recirculating ball bearings (KF), mounted horizontally. An axial kit must be adopted in order to obtain an optimal connection with the electric motor;
- The electric motor is a stepper motor (EMMS-ST) of middle size (M), with straight connector (S) and a displacement encoder (E);

- The controller which must be adapted to the stepper motor (CMMS-ST). The power to be supplied to the whole system corresponds to 48 V at direct current.



Axis:
 ELGC-TB-KF-60
 Axial kit:
 EAMM-A-T42-57A



Motor:
 EMMS-ST-57-M-SE-G2
 No gear



Controller:
 CMMS-ST-C8-7-G2
 Power section
 48 VDC

Figure 3.1.2 – Bowing machine main components.

The load used in the simulation has been calculated with the following requirements: the maximum possible effective stroke equal to 650 mm (which corresponds to the length of a standard violin’s bow), the maximum mass to be moved equal to 2 kg (including the bow and the component for the connection of the frog on the linear drive structure) with no additional external forces and a repetition accuracy of 0.1 mm.

In the simulation run, it has been hypothesised an operational cycle in which the system has to complete the total distance of the stroke (650 mm) and returning to the starting point, with a maximum speed of 1 m/s (as capped in chapter 1.4) and a maximum acceleration of almost 7 m/s²; this second value is relatively high for the standard use of the violin and has been chosen as a conservative value from the Guettler diagrams in Figure 1.3.1. The whole motion profile is depicted in Figure 3.1.3. In the graph, the displacement curve is the black one, the speed corresponds to the blue and the acceleration to the grey one, respectively.

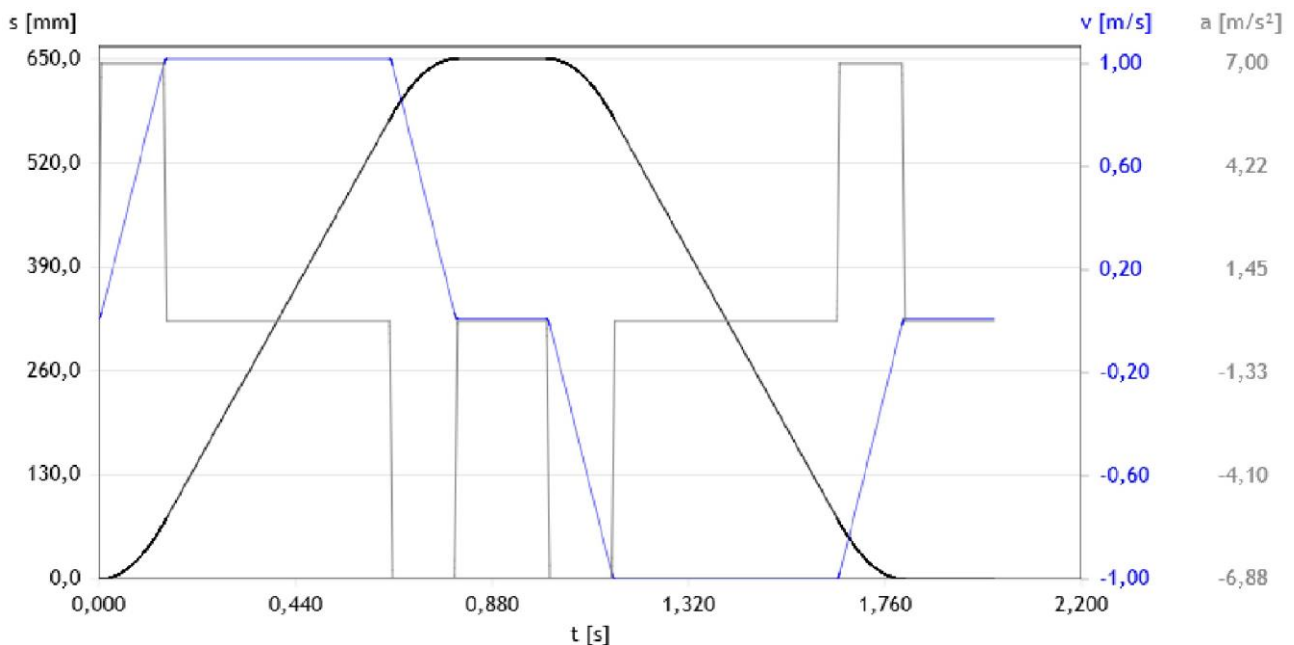


Figure 3.1.3 – Operational motion cycle profile.

From the analysis of the profile above, it results that the whole system takes 2 s in total (1.6 of travel time plus 0.4 s of dwell time) to execute the whole requested cycle with the speed and acceleration input data.

For what concern the stress on the electrical engine, if the cycle is considered as divided into two exact parts (from the origin to the stroke final and back), from the simulation is found that for each part, the torque required from the engine is 0.49 Nm at 769 rpm of revolution; these values fall if the root mean square of the torque and the average speed (respectively 0.259 Nm and 630 rpm) are considered. The two points obtained are then plotted in the motor diagram (from the Festo catalogue), as in Figure 3.1.4, which is a graph that depends on the technical data of each engine and represents the torque an electrical engine could produce as a function of the rotational speed.

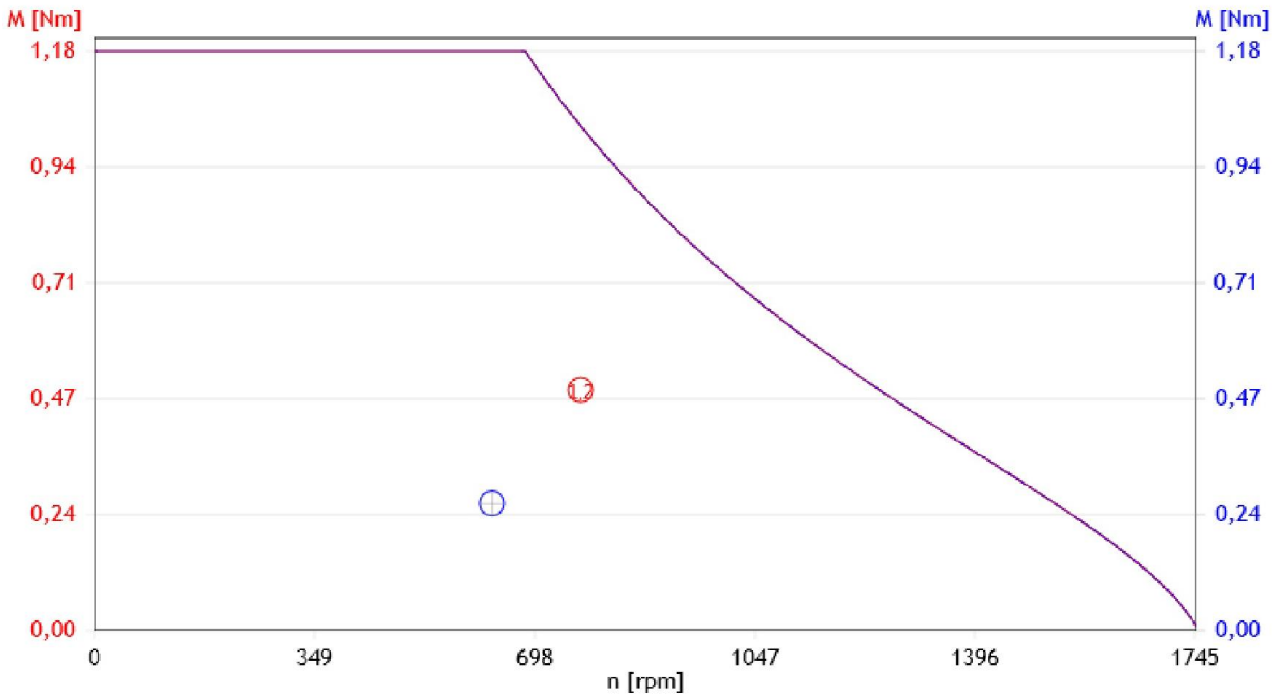


Figure 3.1.4 – Electric motor diagram.

The red dot corresponds to each of the two parts of the cycle (they are exactly the same), while the blue dot corresponds to the average value (rms). As can be noticed, all the points fall far below the curve, which means the requirements coming from the operational simulated cycle can be met safely.

As an overall, the price proposed by Festo for all the components composing the whole system was relatively high (around 3000 €). The point is that, as this project is in its early stages, it is not still sure what kind of developments and eventually profit it could have. That is why, the technical analysis of a bowing machine was performed but not continued for the moment for economic reasons, however it is still an open point for future developments around the subject.

The whole technical data and simulation sheets summarized in the previous pages are available in the Appendix section of this work of thesis.

3.2 Alternative bow frog design analysis

As concluded in the previous chapter, the bowing machine solution was not proceeded, due to the high costs of all the components. What has been considered instead, was to keep the human player

instead of the machine to play the instrument, and modify the frog so that it could be easier to mount some sensors on it in order to measure the actions on the bow and the string, even by losing the repeatability advantage coming from a machine.

In this direction, the work done by Demoucron in 2009 has been of great inspiration for deciding what kind of design should have the new frog had. He and his team designed a sensor for measuring the bow force in normal playing, which was attached to the frog, position where the added weight gives minimum influence on the playing properties of the bow [17]. The sensor was designed as a detachable unit, which could easily be moved to any bow without damaging the frog or the hair. From the constructive details point of view, the force sensor consisted of a thin leaf spring of steel on which two strain gauges were glued, as depicted in Figure 3.2.1.

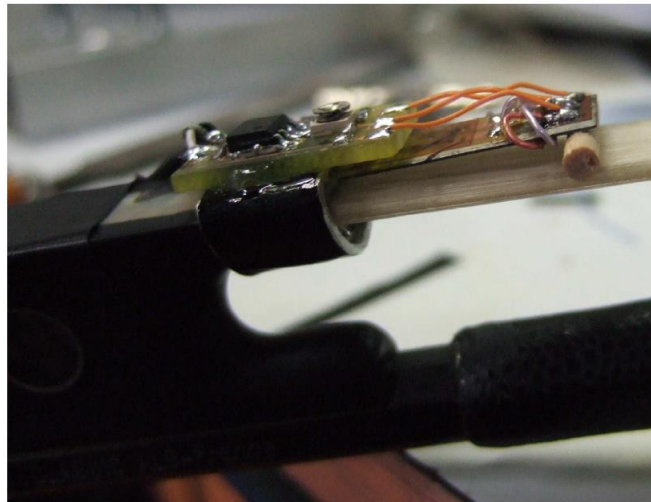


Figure 3.2.1 – Demoucron’s force sensor detail (2009).

The tiny steel plate was fixed to the flat side of the ferrule (which is the part of the bow which keeps the bow hair fixed inside the frog) by a clamping ring. The free end of the strip was in contact with the bow hair through a small cylindrical piece of wood. The bending of the strip generated a signal which gave an accurate estimation of bow force. The strip was mounted on the side of the hair facing the string and thanks to the wooden cylinder it was keeping the hair always under a certain bending static loading condition, which was reducing when the hair were pressed against the violin’s string. A schematic design overview of the frog with the sensor can be appreciated in Figure 3.2.2.

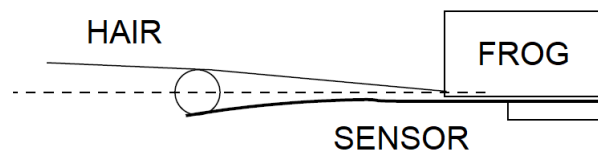


Figure 3.2.2 – Schematic Demoucron’s bow force sensor.

So, it has been observed that it is important to have a flexible element (the steel plate) which has to be in contact with the bow hair that bend at contact with the string. Moreover, the frog has to keep its properties of keeping the bow hair as tighten as possible.

The first step in the realization of the new bow frog has been to remove one from a standard bow, observe the shape and obtain the geometrical dimensions. It has been noticed that the plates, which are going to host the sensors, are going to be two (not only one as in the case of Demoucron’s); one for the normal direction (with respect to the bow and string axes) and the second one for the axial

direction, corresponding to the axis of the bow. The addition of the latter has been decided for a matter of completion, in order to consider also the friction contribution and the action performed by the player. As indicated in Figure 3.2.3, the position of the plates in the frog has been highlighted in yellow, while the cuts that shall be manufactured in order to host the plates are indicated in red.

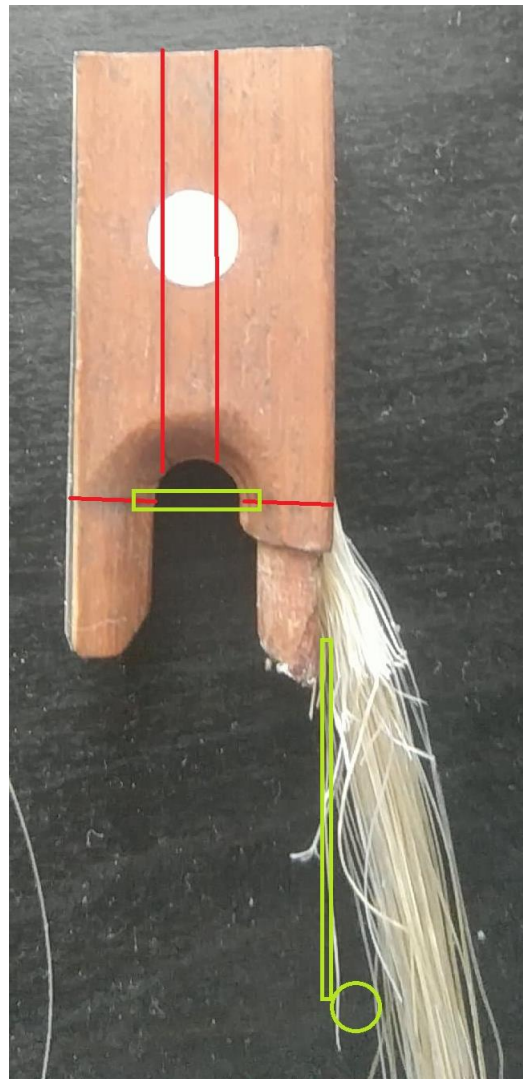


Figure 3.2.3 – Plates position in yellow and manufacturing cuts in red.

A first design of the frog has been realized with the software Solidworks and shown in Figure 3.2.4. In a second step, for manufacturing reasons, the shape has been optimised in a more prismatic way, as shown in Figure 3.2.6. This one, represents the final design. The final design of the new bow is shown in Figure 3.2.5

The use of screws makes the whole device adaptable to any bow. The bigger hole on the rear part has been designed in order to keep the functionality of the frog, since is where the hair have to pass through, and then being blocked with a cap in order to keep them straightened.

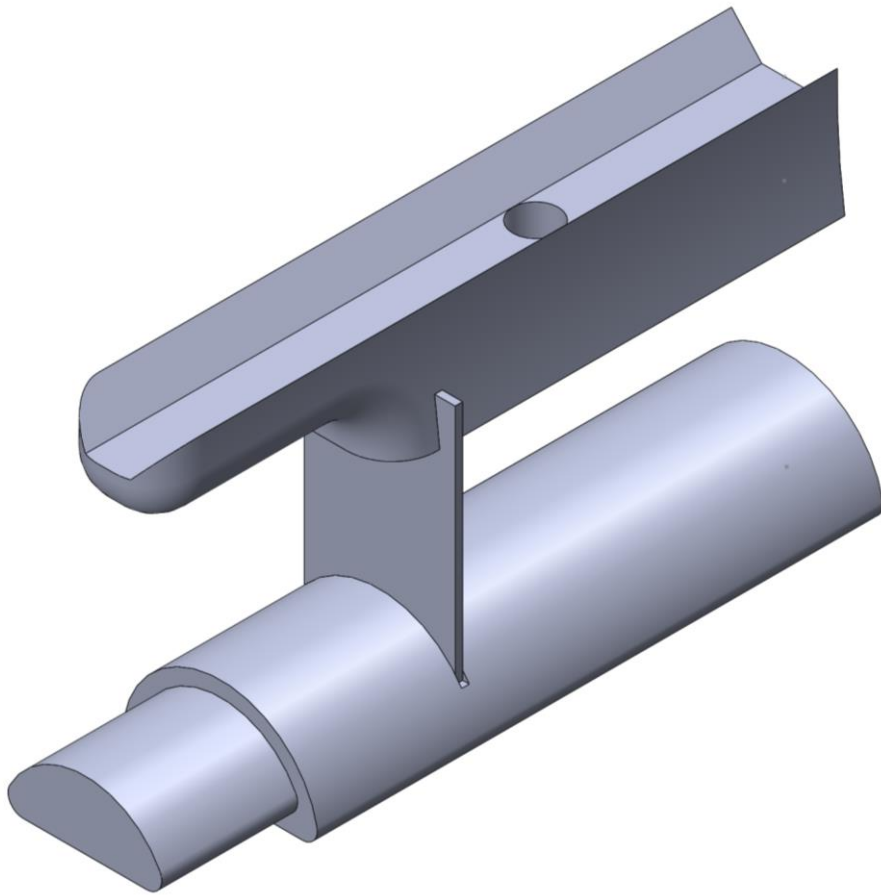


Figure 3.2.4 – First design of the new frog.



Figure 3.2.5 – New bow design overview.

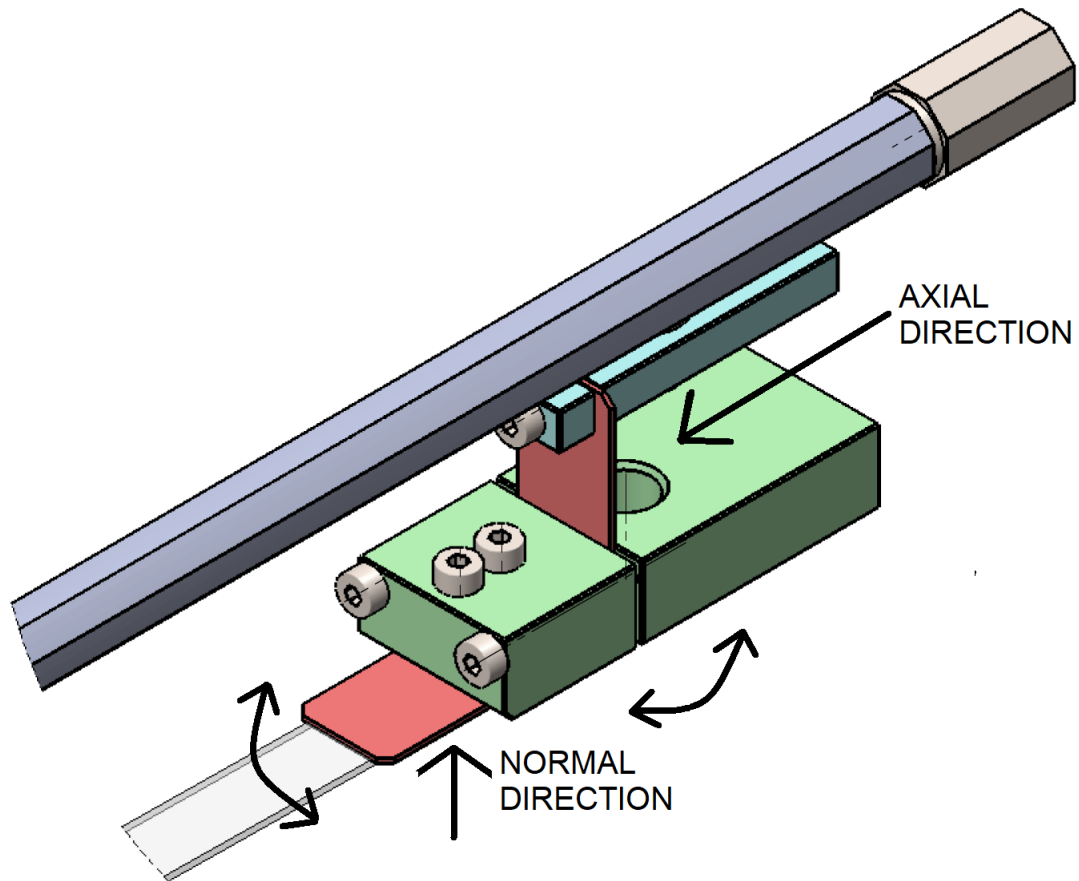


Figure 3.2.6 – New frog design overview, with sensors directions and plates rotations.

Calculations on the loads, forces and deformations have been performed on the two plates. Some assumptions have been done: the axial force has been assumed as equal to 100 N (considering frictions and the player's gesture) and the normal is equal to 5 N; both values are overestimating the actions in a real case. The chosen material for the plates is steel which holds the well-known mechanical properties (Young modulus E equal to $2 \cdot 10^5$ MPa, density is 7800 kg/m^3 and Poisson coefficient 0.3). The bending load M_f has been evaluated as:

$$M_f = F \cdot l$$

where l is the length of the plate, corresponding to the arm of the force F (either axial or normal). The tensions σ and deformations ε are respectively equal to:

$$\sigma = M_f \cdot W_f$$

$$\varepsilon = \frac{\sigma}{E}$$

where the resistance modulus W_f has been evaluated, for a prismatic solid, as:

$$W_f = \frac{b \cdot h^2}{6}$$

which contains the geometrical width b and thickness h of the plate. The final calculations for both plates are listed below in Table 3.2.2.

Table 3.2.1 – Geometrical properties of the frog’s plates.

Geometry	Axial Plate	Normal Plate
l , length [mm]	19.5	22
b , width [mm]	10	10
h , height [mm]	0.5	0.5
W_f , resistance modulus [mm ³]	0.42	0.42

Table 3.2.2 – Loads, tensions and deformations on plates.

Property	Axial Plate	Normal Plate
F , force [N]	100	5
M_f , bending moment [Nmm]	1950	110
σ , bending stress [MPa]	4680	264
ε , bending deformation [%]	2.34	0.13

Always refer to Figure 3.2.6 for the directions of the forces acting on the plates.

In conclusion, the new frog has been built in aluminium by the manufacturing company OCMA of Gianluca Esposito, in Turin. The final result is shown in Figure 3.2.7 and Figure 3.2.8.

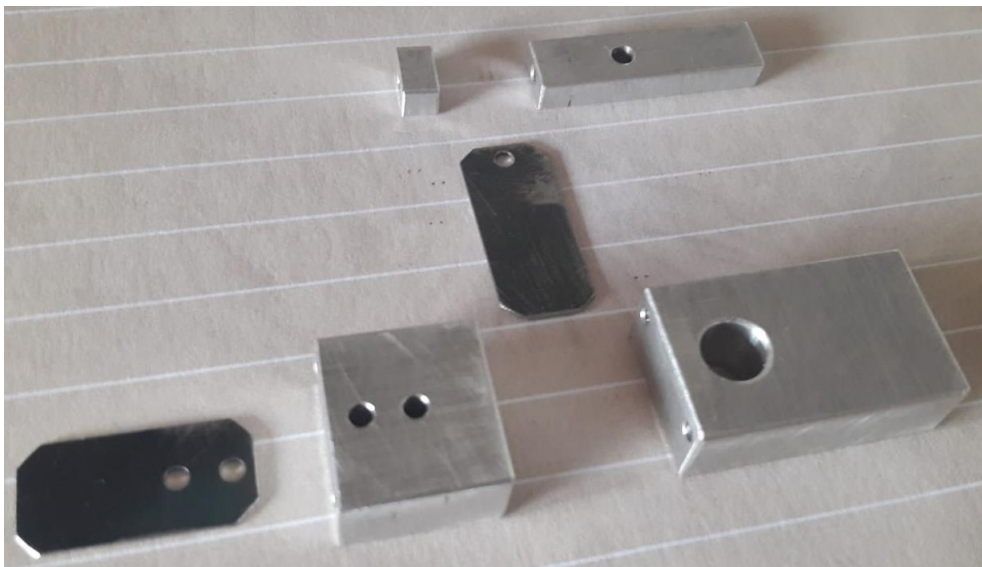


Figure 3.2.7 – New frog final result (1).



Figure 3.2.8 – New frog final result (2).

4. Frame capture technique for bow velocity evaluation

In the final chapter of this work of thesis, after having analysed an alternative design for the bow frog, it will be discussed a technique that allows the frame capture of the player's gesture (only visual).

As mentioned in chapter 1.5, one of the main parameters considered to evaluate the bowing gesture, is the velocity of the bow. In order to obtain this information, it has been adopted a particular Matlab script, developed in 2014 by Elvio Bonisoli for the study of the dynamics of the Levitron (a particular kind of magnetic spinning top), and adapted for this particular case of study.

In the first step of the procedure, the player has been recorded using a camera in the act of playing the instrument (in this case an ukulele has been used instead of a violin, but the final result is not affected).

Before the image has been acquired, the bow's appearance had been modified: the bow stick made of wood (brownish colour) has been covered with some white paper and the tip with black tape; in this setup it is very important that the player performs in front of a plain white wall and that the camera is placed exactly in front of him/her, in order to create the maximum possible contrast (the reason will be shortly explained). The experimental setup, with the main directions of displacements is shown in Figure 4.1. In this way, the bow is studied while moving in the y-z plane.

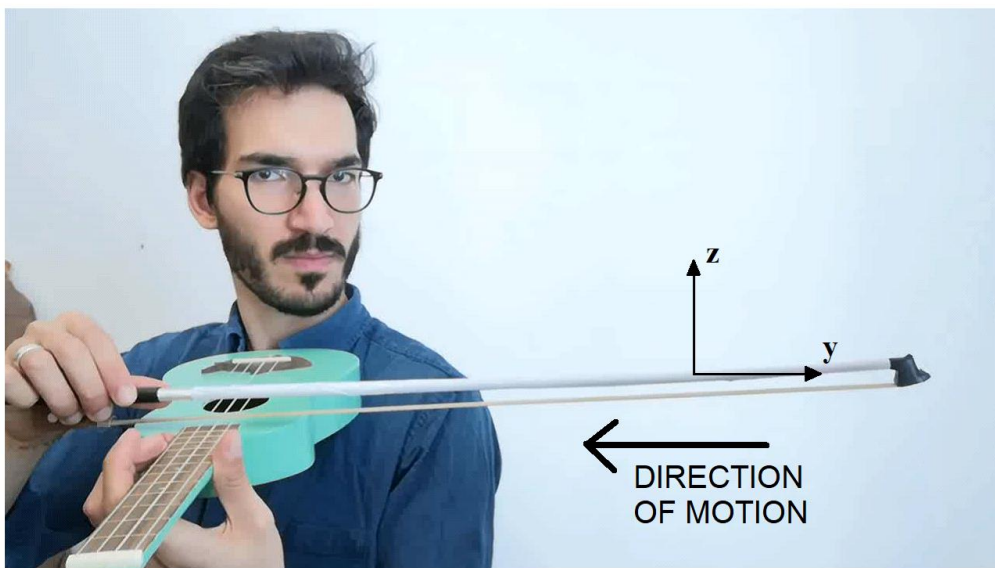


Figure 4.1 – Experimental image acquiring setup.

Once the video has been recorded, the script in Matlab must be launched and the video uploaded; the script starts modifying the image, by looking for the best available contrast conditions (in black and white), as shown in Figure 4.2.

After asking whether the level of contrast is acceptable or not, it is required to select the area of interest (red window in picture below) for the frame acquisition. Then the contrast is inverted in order to have the body to study (bow's tip), which was initially in black, in white colour over a black background, like in Figure 4.3. That now explains why a black tape has been initially applied on the bow tip and the stick covered in white.



Figure 4.2 – Modified video with automatic level of contrast.



Figure 4.3 – Window of interest with inverted colours.

Now, the centre of gravity of the tip (the white body), is evaluated frame by frame, always inside the selected window. Actually, the script only considers the white pixels of the image, which means it must be avoid as much as possible any kind of interference with the body of interest (like the player or the bow's stick and hair).

Due to its definition, the centre of gravity is equal to:

$$y_G = \frac{S_z}{A} \quad z_G = \frac{S_y}{A}$$

where S is the first moment of area with respect to the reference system and the specific axis and A the relative area. So, the centre of gravity is calculated by summing up all the white pixels frame by frame of the whole acquired movement; that is the reason why it is required to study an image with the highest possible level of contrast. The barycentre can be appreciated in Figure 4.4 (indicated with a red circle), which represents also the last frame analysed by the script.



Figure 4.4 – Centre of gravity in red in the last frame of the motion.

After that, all the information acquired by the barycentre displacement of the bow's tip in the y-z plane are summed up and plotted. The results are shown in the next figures.

In the video considered, the direction of the bow was inwardly with respect to the position of the instrument (from right to left of the screen, as indicated by the arrow in Figure 4.1), and that is why the value of speed along the y-axis in Figure 4.7 assumes a negative value, having set the positive direction of y outwardly (from left to right). Moreover, the blue line represents the instantaneous value of velocity, while the dashed red line represents the average value.

In Figure 4.5, it can be appreciated the bow tip trajectory, where every blue dot represents the position of the barycentre in each frame, and the blue line interpolates all these points. It can be noticed how the trajectory of the bow was not straight, but there were some small oscillations (up and down) in the range of -20 mm and $+20$ mm (as shown in Figure 4.6); that is why, later on in the pictures (Figure 4.8), the speed in the z direction oscillates from negative to positive as well.

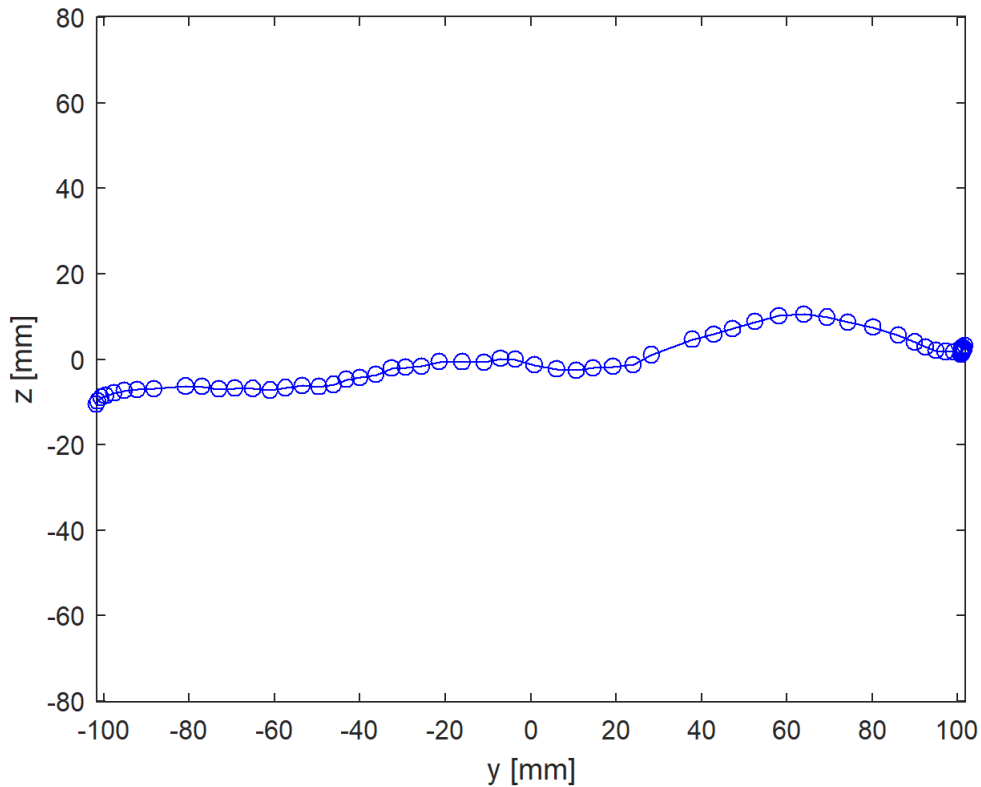


Figure 4.5 – Bow tip trajectory.

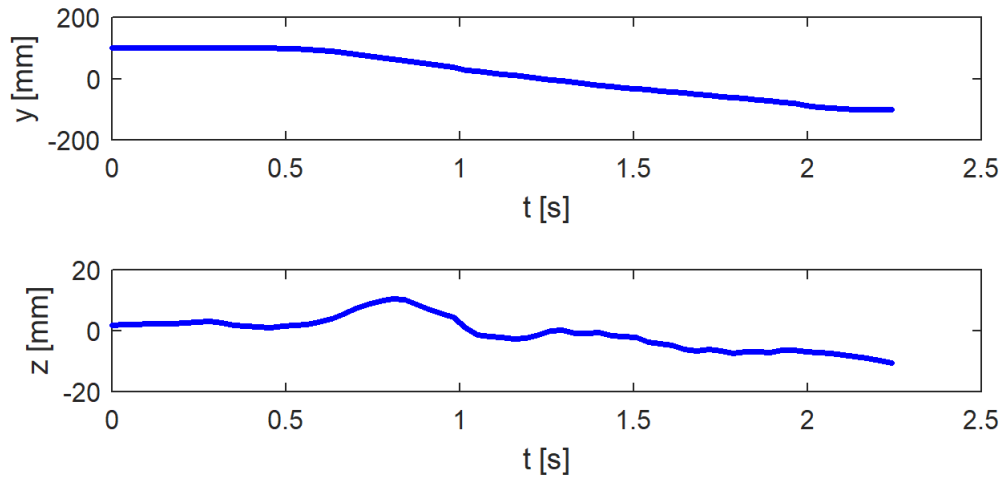


Figure 4.6 – Bow tip displacement along the main axes' directions.

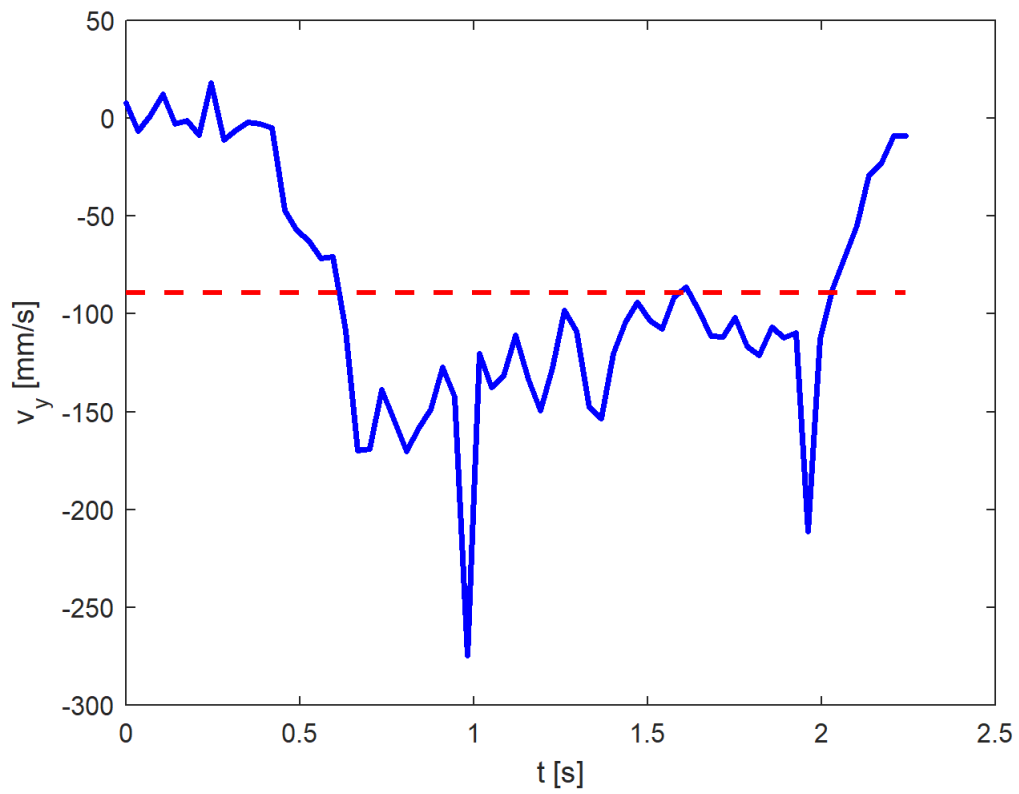


Figure 4.7 – Bow velocity along y-axis.

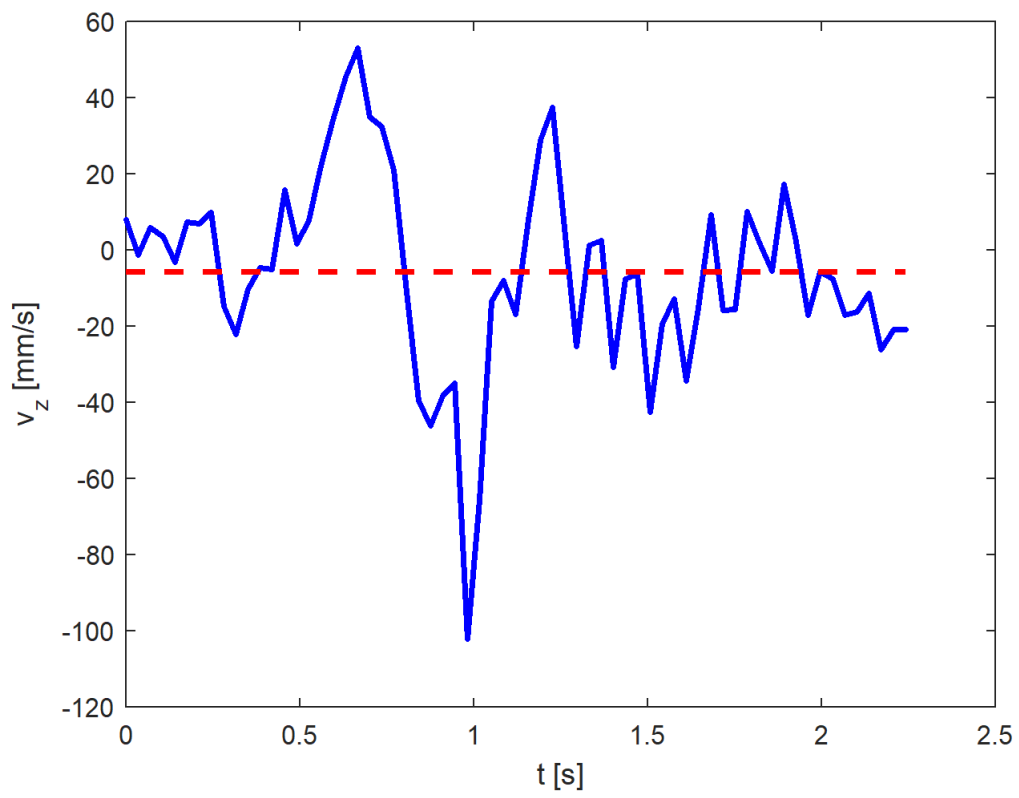


Figure 4.8 – Bow velocity along z-axis.

Conclusions

In conclusion, many topics have been covered in these pages. First of all, the state of the art and some interesting theories about the bowed string and the stick-slip motion have been presented. It is clear that the most important parameters influencing this phenomenon are the bow velocity, force and bow-bridge distance. Also, acceleration plays a minor role. Some more research on the influence of friction, damping and tilting angle would complete the picture about the physics and get a closer description of a real case.

Later on, the description how to build a modern controlled bowing machine is definitely an interesting matter of discussion and future developments, even if it has not been built yet (for economic reason). A bowing machine would allow to have the repeatability advantage in the testing of the acoustic performance of the stringed instrument. An alternative but at the same time concordant solution is the new designed removable bow's frog, which would allow the measurement of accelerations and forces in two directions (normal and axial) with the use of strain gauges yet not compromising the lightness and flexibility of the original bow.

With the last chapter, also the graphical side of the topic has been covered, which leaves the only important matter on the acoustic performance of the instrument. The latter has to be the natural prosecution of this work of thesis for those who will have the duty (and hopefully the intellectual pleasure I had) of continuing the research in this direction.

Appendix

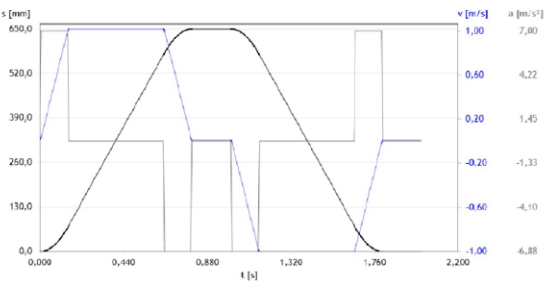
Positioning Solution proposal for positioning drives



PositioningDrives
Version 2.3.24
13/03/2019

		
Axis: ELGC-TB-KF-60 Axial kit: EAMM-A-T42-57A	Motor: EMMS-ST-57-M-SE-G2 No gear	Controller: CMMS-ST-C8-7-G2 Power section 48 VDC

Technical data		Load calculated from:	
Axis technology	Toothed belt	Max. possible Effective	Required 650 mm
Guide	Ball bearing	Repetition accuracy	0,1 mm
Motor type	ServoLite	Maximum moving mass	2 kg
Maximum ambient air temperature	25 °C	Additional external force	0 N
Mounting position, Axis	Horizontal 0 °		

This solution offers you the following performance		Motion profile see diagram (Detailed motion profile, Complete)
Travel time	1,605 s	
Cycle time	2,005 s	
Dwell time	0,4 s	
Load Axis	15 %	
Load Motor	48 %	
Load Guide	41 %	
Distance of load		
Mounting position, Axis	Horizontal 0 °	
Mounting position, Guide	Up or down	
m = 2 kg	F = 0 N	
X 650 mm		
Y 0 mm		
Z 200 mm		

Please ensure that the following dynamic values the dimensioning is based on do not exceed the limit values of your equipment: Axis Speed: 1 m/s, Acceleration: 6,878 m/s², Deceleration: 6,878 m/s²

Festo does not guarantee the suitability of any equipment ordered pursuant to the use of this software for any particular purpose unless that purpose has been fully explained to Festo.
Moreover, this software should not be relied upon for the determination of any characteristics which can be otherwise independently verified.
Festo cannot be held liable for claims due to failure to achieve the calculated results, including the case of errors in calculation.
- The right to make changes is always reserved -

Positioning Bill of materials

	Part No.	Amount	Unit	Order code	Designation
1	8062780	1	PCS	ELGC-TB-KF-60-800	Linear drive
2	4327034	1	PCS	EAMM-A-T42-57A	Axial kit
3	1370479	1	PCS	EMMS-ST-57-M-SE-G2	Stepper motor
4	572211	1	PCS	CMMS-ST-C8-7-G2	Controller
5	8001376	1	PCS	NEBC-S1G25-K-5.0-N-S1G25	connecting cable
6	550749	1	PCS	NEBM-M12G8-E-10-S1G9	encoder cable

Do not forget

Power supply
Cable
Sensors
Assembly accessories

Positioning Bill of materials



PositioningDrives
Version 2.3.24
13/03/2019

Axis	ELGC	Gantry	Motor	EMMS-ST	Stepper motor
	TB	Toothed belt		57	Flange size
	KF	Ball bearing guide		M	Size, middle
	60	Size		S	Straight connector
	800	Stroke [mm]		E	Displacement encoder
				G2	Series

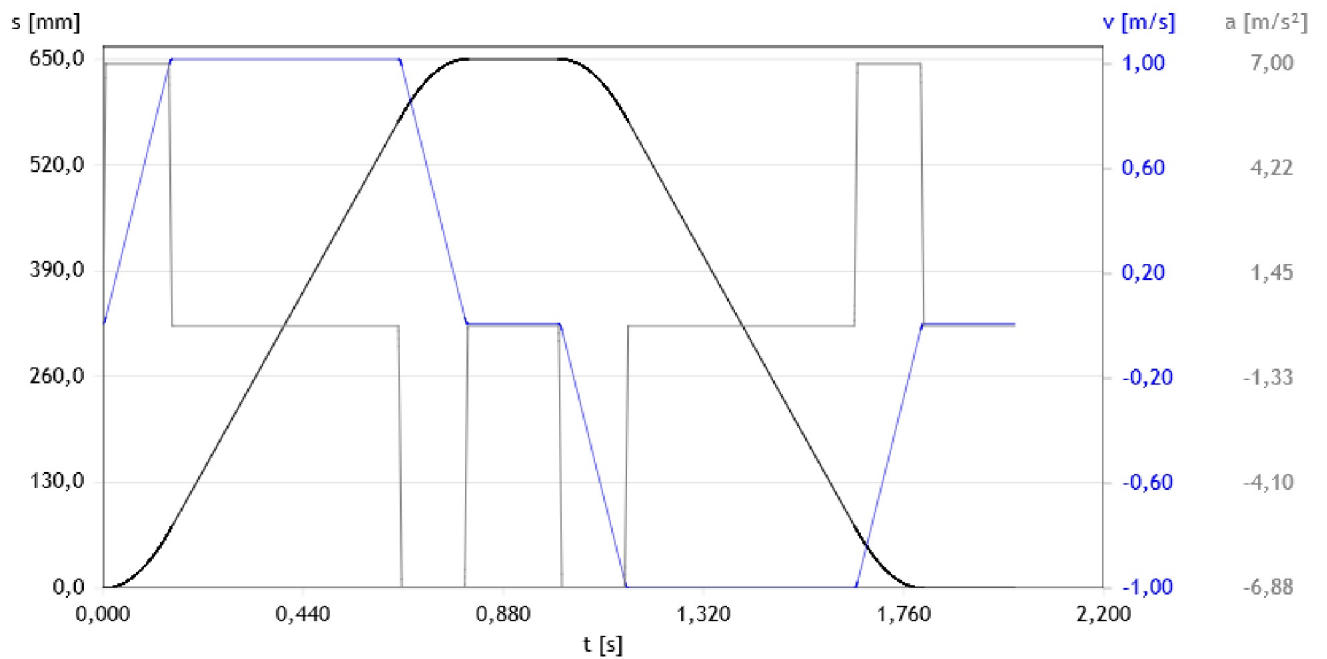
Positioning Results diagrams



PositioningDrives
Version 2.3.24
13/03/2019

Detailed motion profile, Complete

Total		Maximum	
Travel time	1,605 s	Speed	1 m/s
Cycle time	2,005 s	Acceleration	6,878 m/s ²
Dwell time	0,4 s	Deceleration	6,878 m/s ²



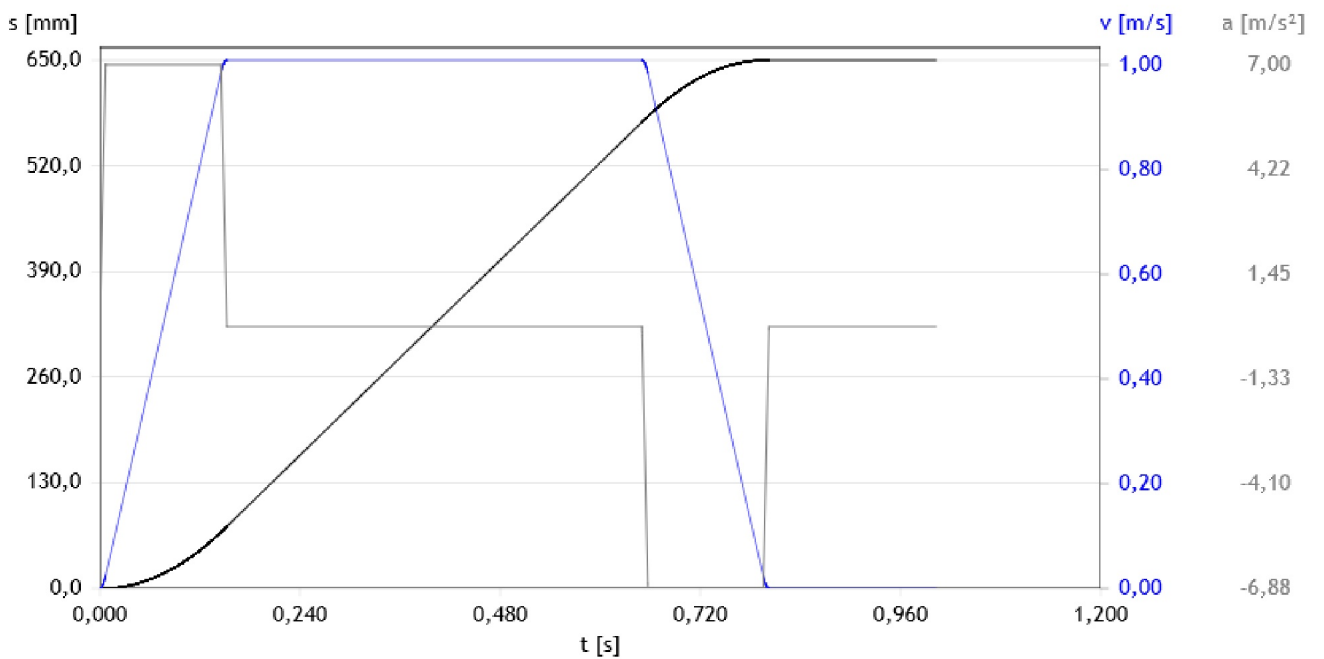
Positioning Results diagrams, Details



PositioningDrives
Version 2.3.24
13/03/2019

Motion profile Step 1

		Maximum	
Travel time	0,802 s	Speed	1 m/s
Cycle time	1,002 s	Acceleration	6,878 m/s ²
Dwell time	0,2 s	Deceleration	6,878 m/s ²



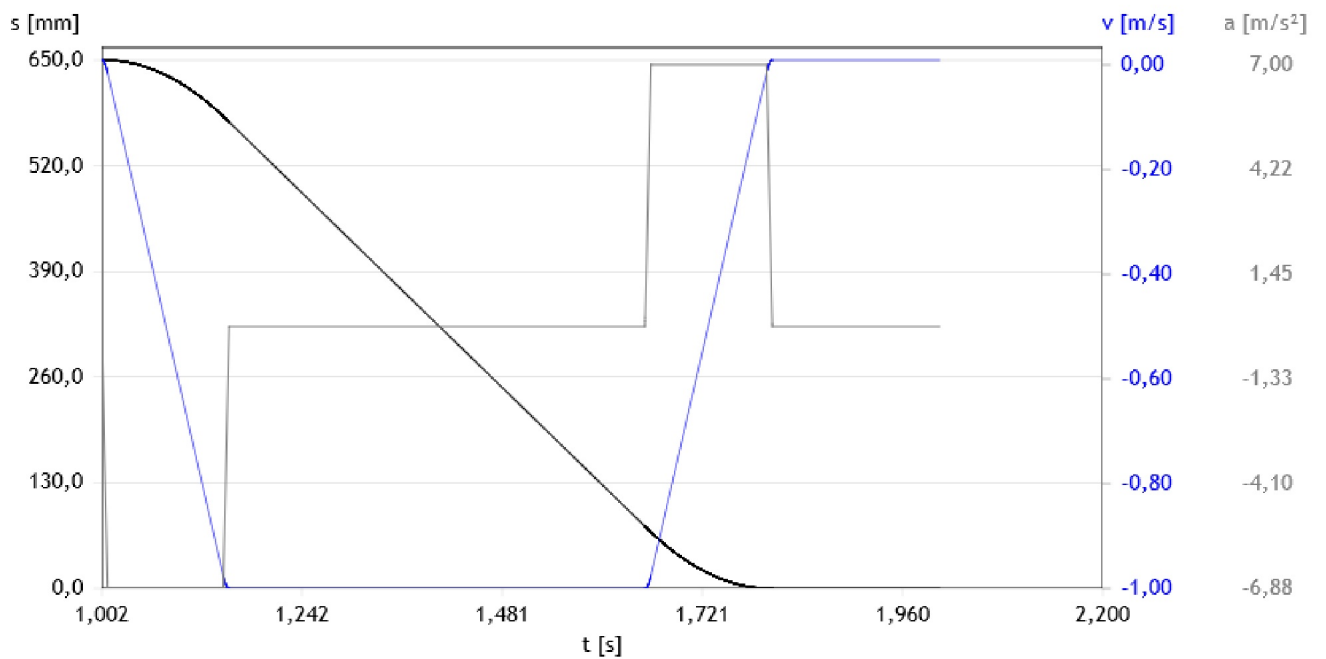
Positioning Results diagrams, Details



PositioningDrives
Version 2.3.24
13/03/2019

Motion profile Step 2

		Maximum	
Travel time	0,802 s	Speed	1 m/s
Cycle time	1,002 s	Acceleration	6,878 m/s ²
Dwell time	0,2 s	Deceleration	6,878 m/s ²

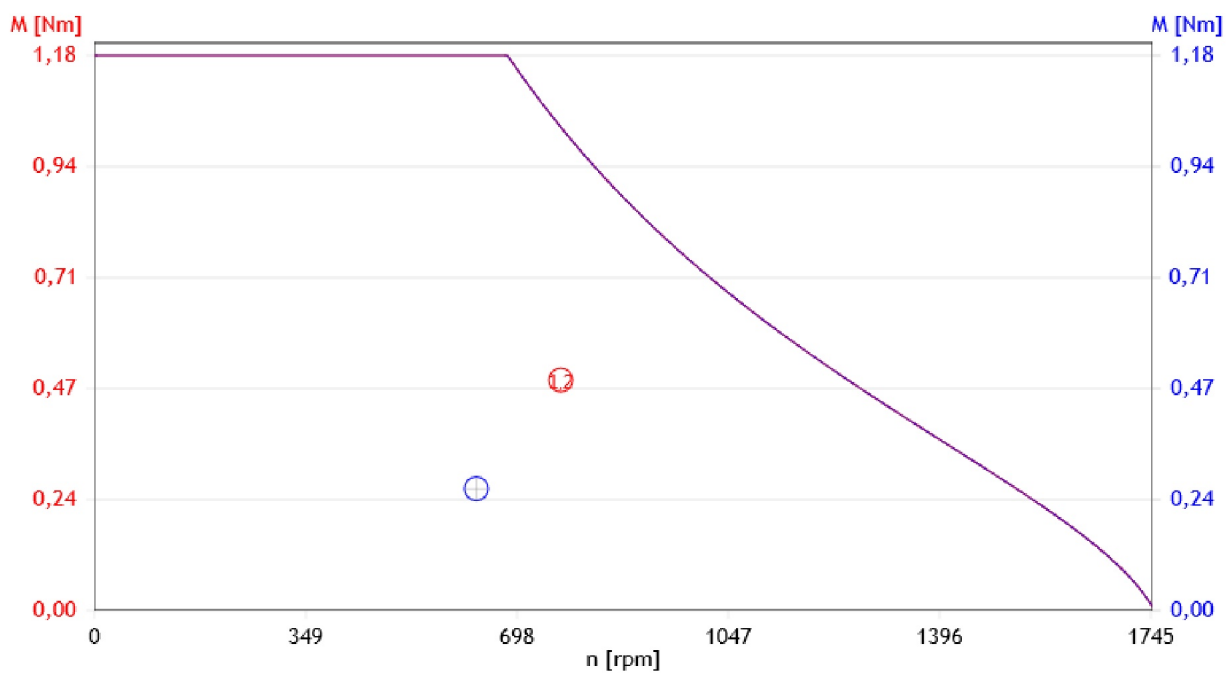


Positioning Motor Diagram



PositioningDrives
Version 2.3.24
13/03/2019

Average speed 630 rpm
Root mean square of torque (Dynamic data) 0,259 Nm



Mp-Step-No.:	Torque	Revolution
1	0,490 Nm	769 rpm
2	0,490 Nm	769 rpm

Positioning Dynamic data



PositioningDrives
Version 2.3.24
13/03/2019

Axis

Type	ELGC-TB-KF-60-800
Calculated maximum speed	1 m/s
Calculated maximum acceleration	6,878 m/s ²
Maximum jerk	985 m/s ³
Required usable force	16,9 N

Shaft extension mounting kit Motor

Maximum pinion revolution	769 rpm
Peak torque Pinion	0,45 Nm
Displacement during emergency stop	33,333 mm
Deceleration Max. possible = 15 m/s ² (Worst case with "Calculated maximum speed")	

Motor

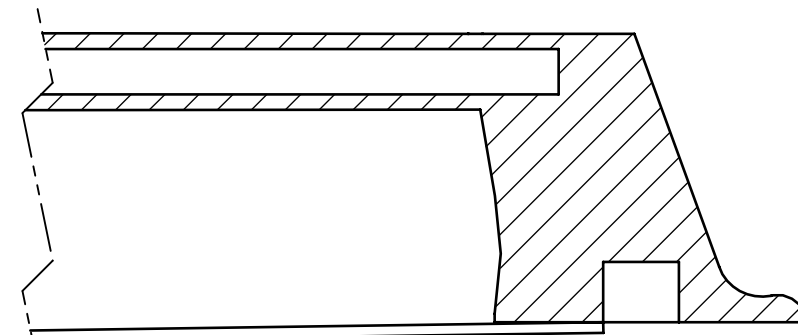
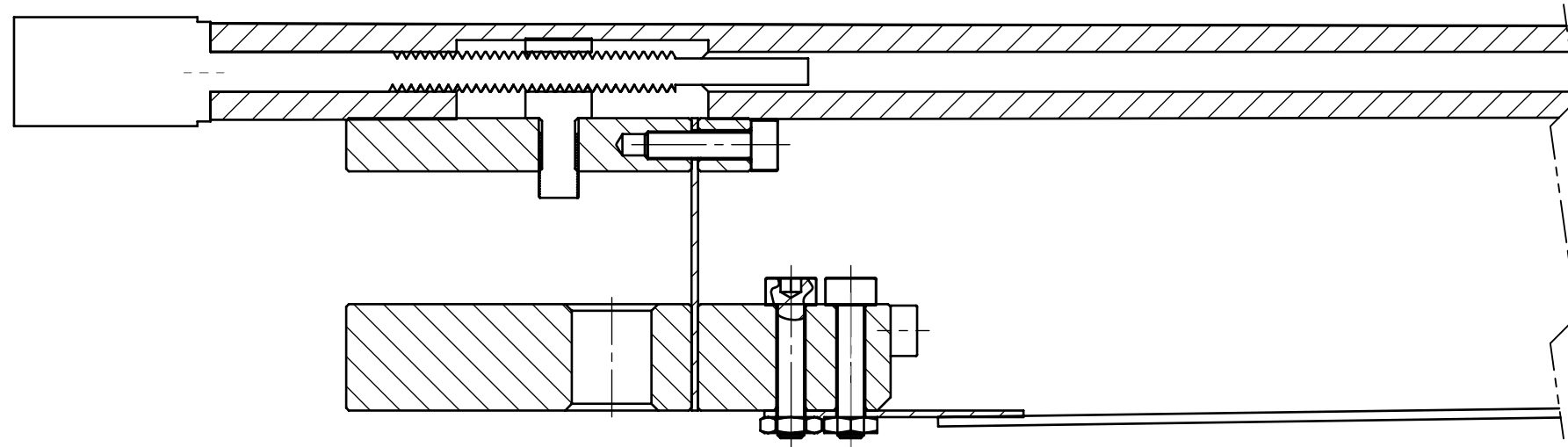
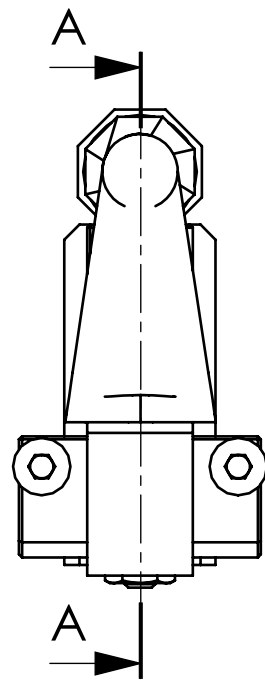
Type	EMMS-ST-57-M-SE-G2
Maximum motor revolution (Cable length = 10 m)	769 rpm
Acceleration torque	0,49 Nm
External torque + Friction	0,25 Nm
Controller voltage stepper motor	48 V DC
Calculated maximum power	62 W
Calculated maximum current	2,1 A
Current for emergency stop	1,2 A
Mass moment of inertia	
Translatory	3,844 kgcm ²
Rotatory	0,094 kgcm ²
External moment of inertia with respect to motor	3,938 kgcm ²
Moment of inertia ratio	9,204

Positioning Product data

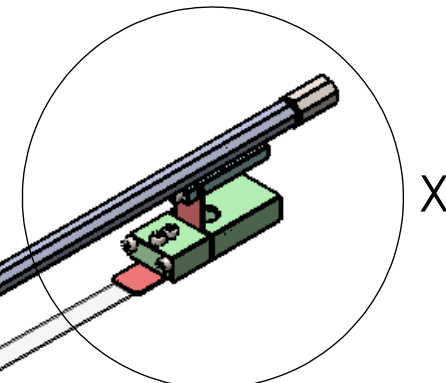


PositioningDrives
Version 2.3.24
13/03/2019

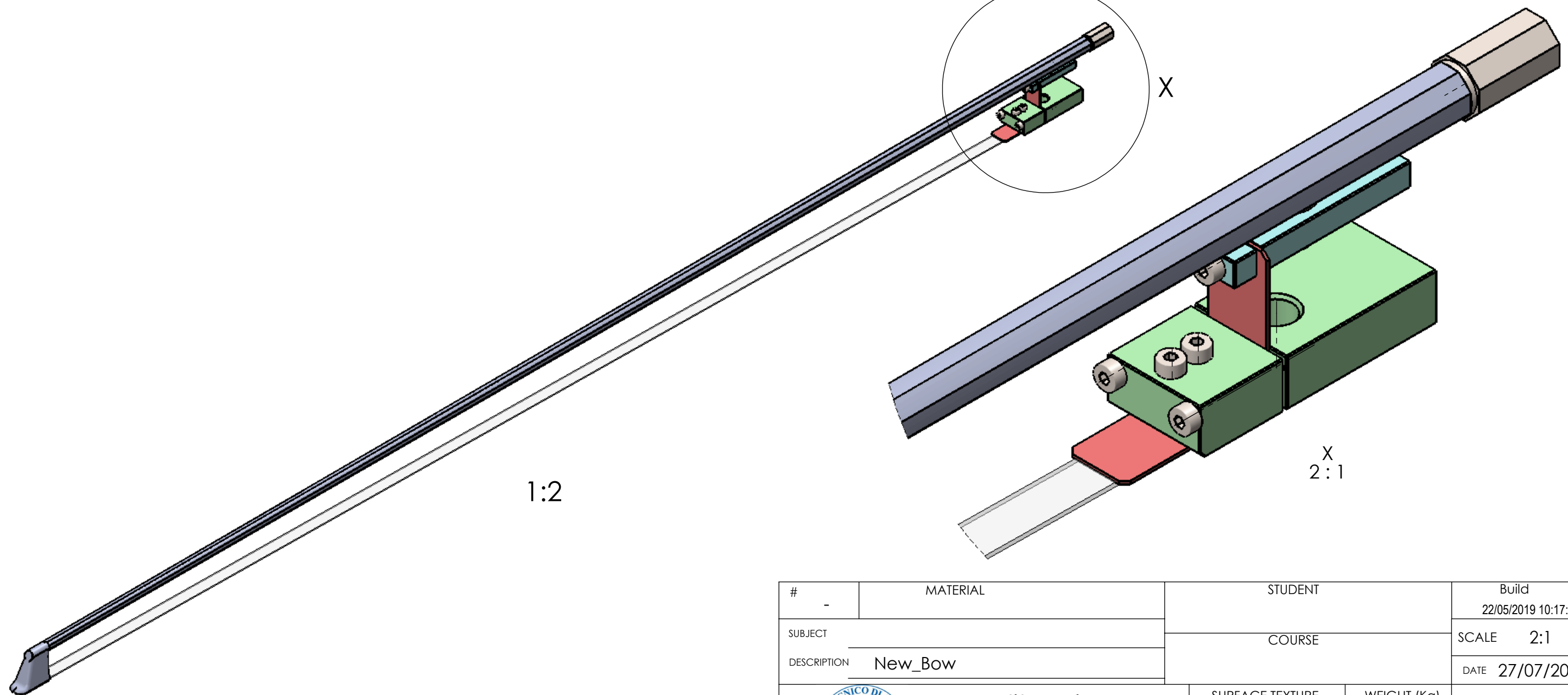
Axis	ELGC-TB-KF-60-800
Max. possible Effective stroke	2000 mm
Repetition accuracy	0,08 mm
Usable force (Limit for project planning)	120 N
Maximum acceleration	15 m/s ²
Maximum speed	1,5 m/s
Mass moment of inertia (Translatory; Moving mass of axis)	0,761 kgcm ²
Pinion	
Feed constant	78 mm
Maximum torque	1,77 Nm
Mass moment of inertia	0,062 kgcm ²
Motor	EMMS-ST-57-M-SE-G2
Maximum speed (Max. Voltage = 48 V)	1940 rpm
Holding torque	1,4 Nm
Rated current	5 A
Mass moment of inertia	0,48 kgcm ²
Maximum ambient air temperature	50 °C
Controller	CMMS-ST-C8-7-G2
Supply voltage	
Logic section	24 V DC
Power section	24 ... 48 V DC
Rated current	8 A
Peak current	12 A



A-A



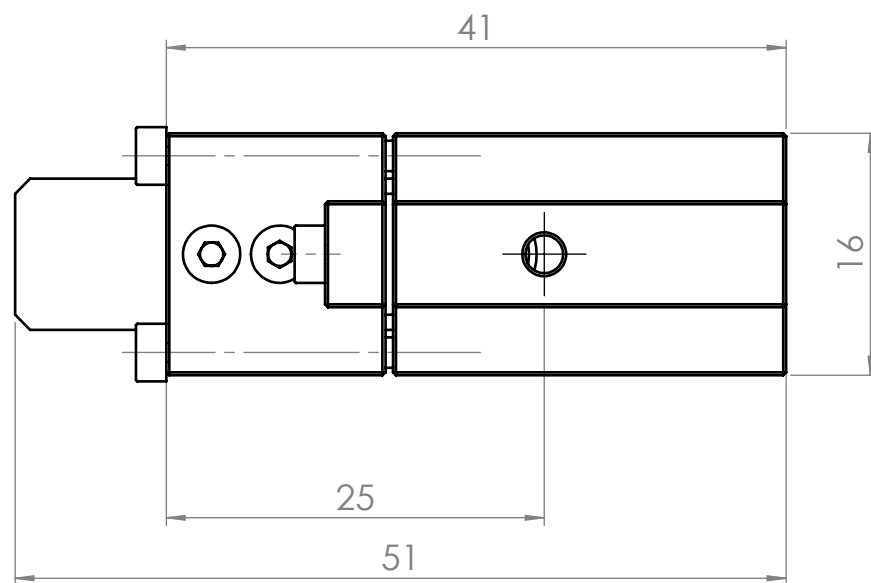
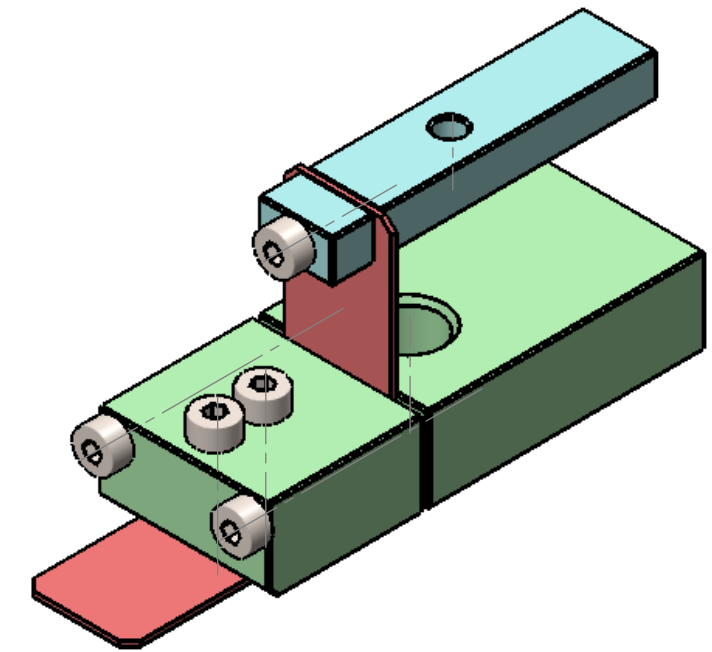
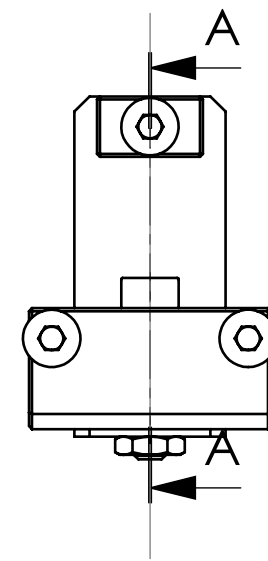
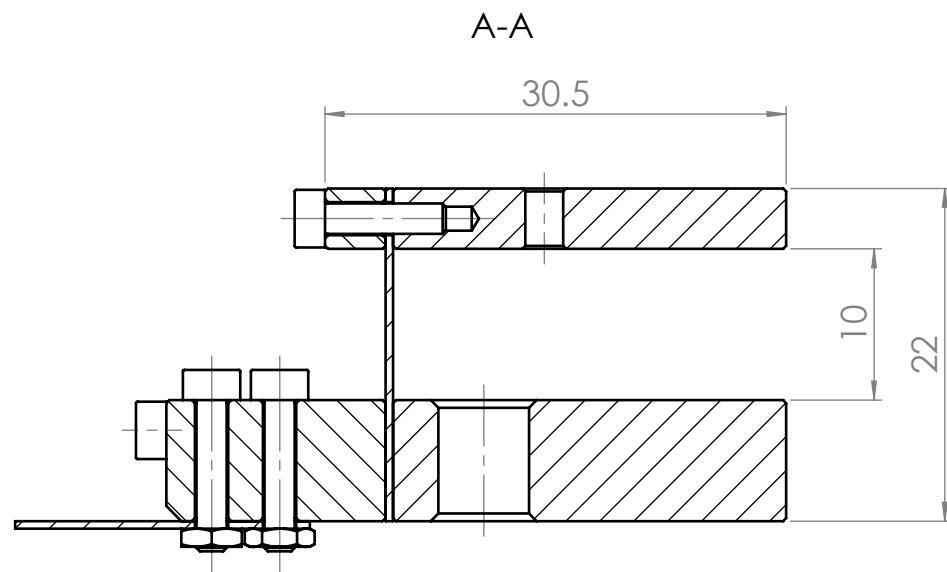
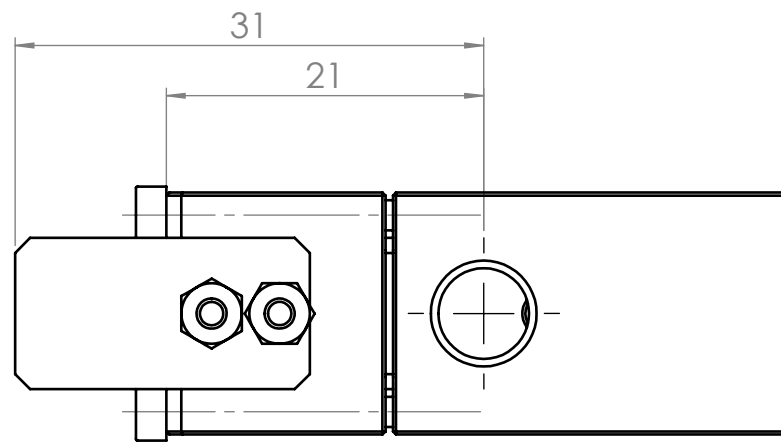
X



1:2

X
2:1

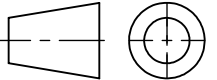
#	MATERIAL	STUDENT	Build 22/05/2019 10:17:54
SUBJECT		COURSE	SCALE 2:1
DESCRIPTION	New_Bow		DATE 27/07/2019
	Politecnico di Torino	SURFACE TEXTURE 	WEIGHT (Kg)
		PAPER A3 1/1	Drawing N.
Politecnico di Torino - Corso Duca degli Abruzzi, 24 - 10129 TORINO			

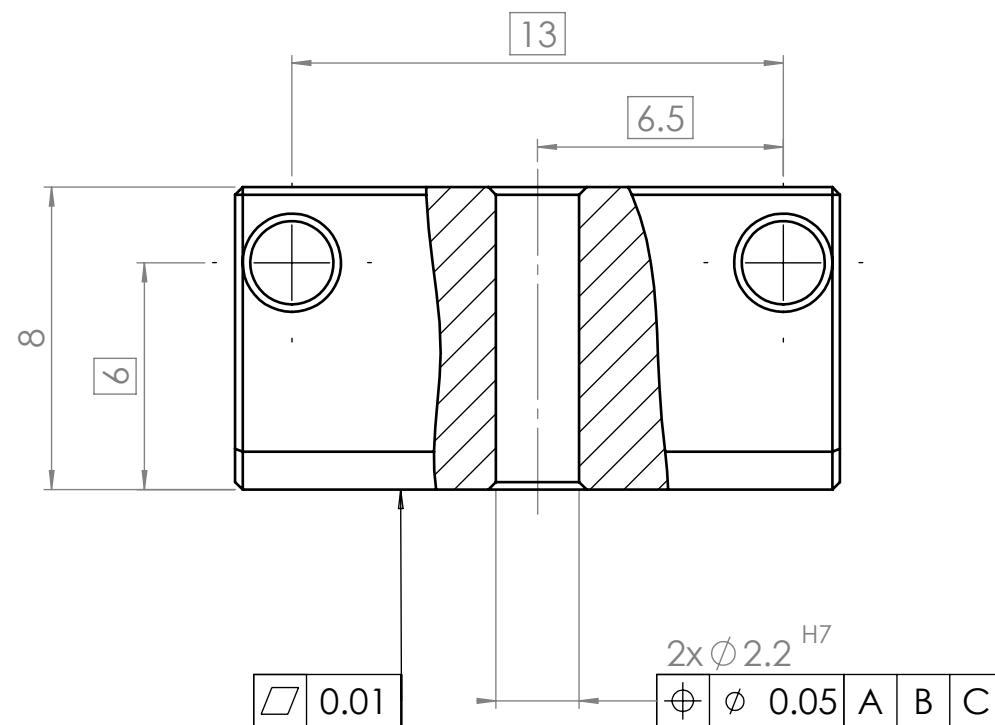
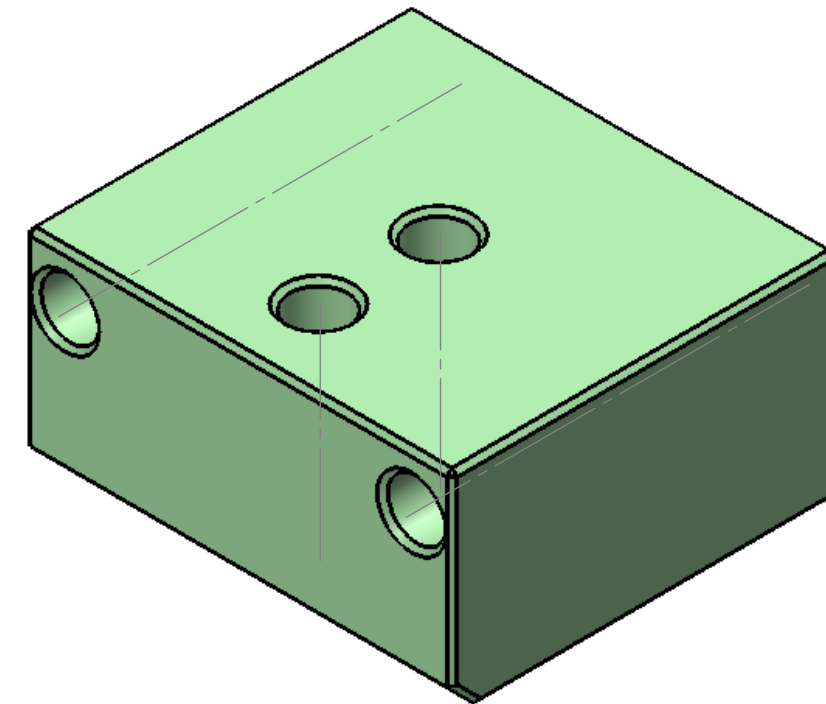
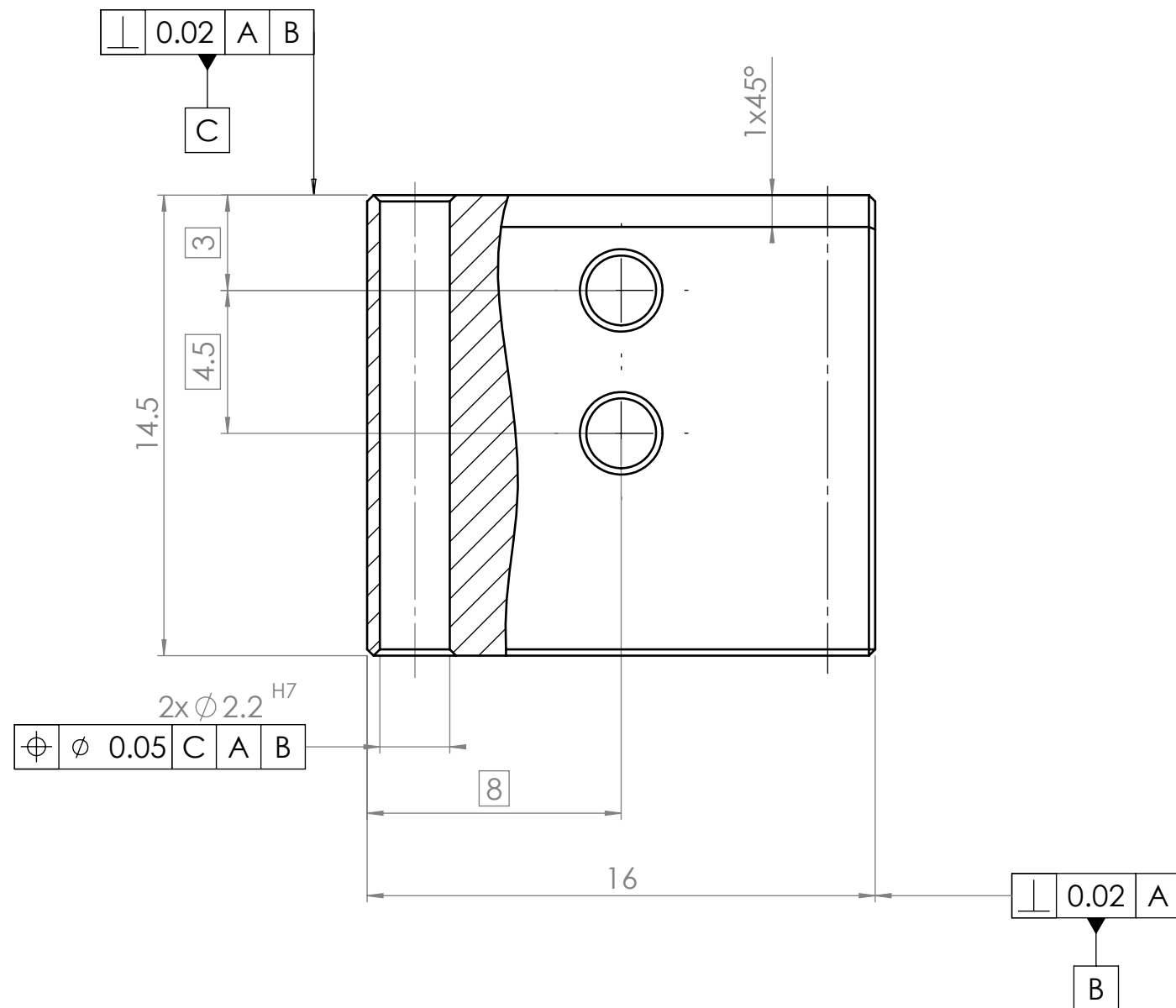


Independence criterion ISO 8015
General tolerances UNI EN 22768-mK

Chamfer 0.2x45°

$\sqrt{Ra\ 0.8}$

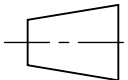
#	MATERIAL	STUDENT	Build
-			03/05/2019 13:45:27
SUBJECT		COURSE	SCALE 2:1
DESCRIPTION	New_Frog		DATE 27/07/2019
 Politecnico di Torino	SURFACE TEXTURE	WEIGHT (Kg)	
	 PAPER A3 1/1	Drawing N.	
Politecnico di Torino - Corso Duca degli Abruzzi, 24 - 10129 TORINO			



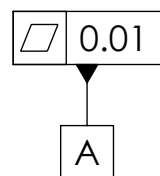
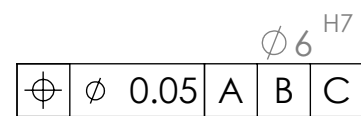
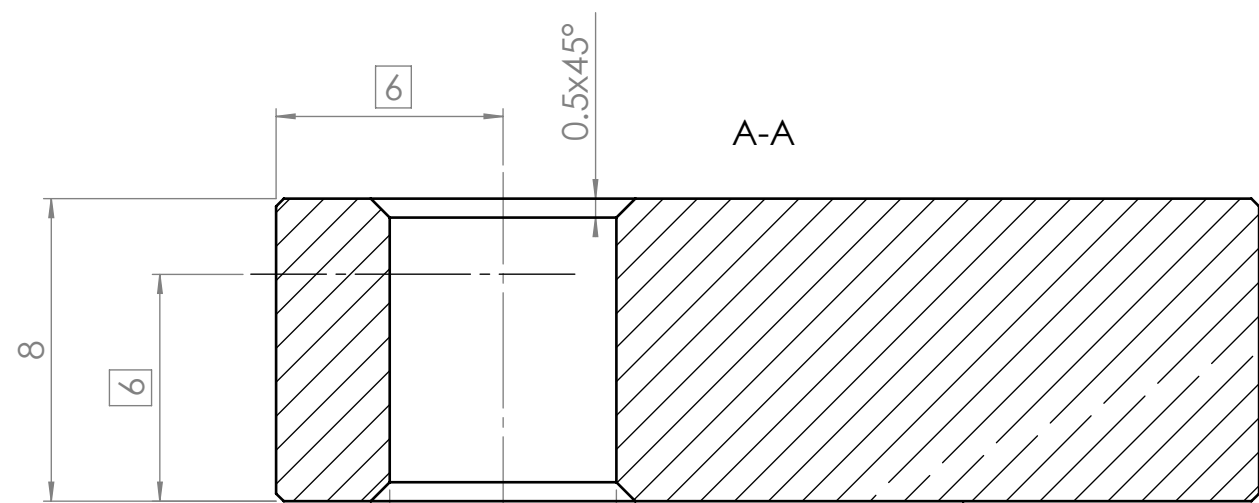
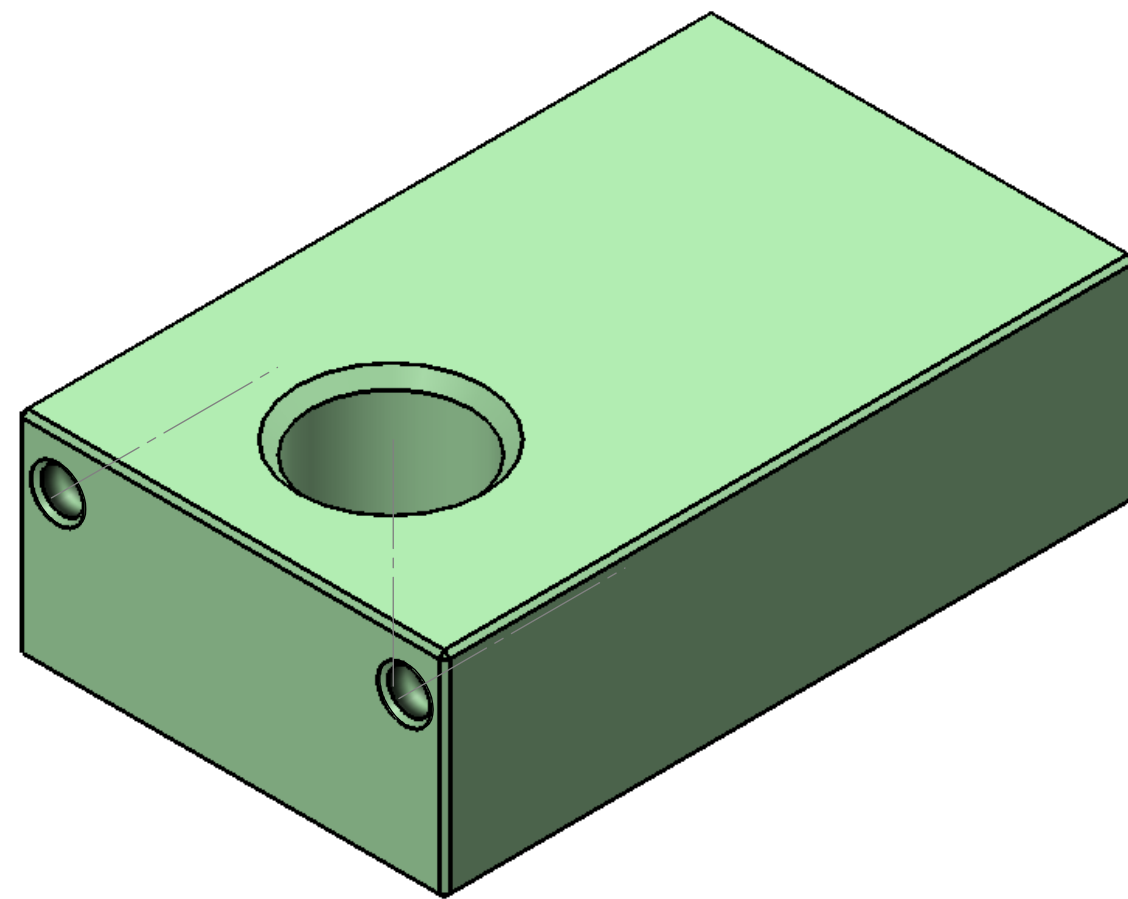
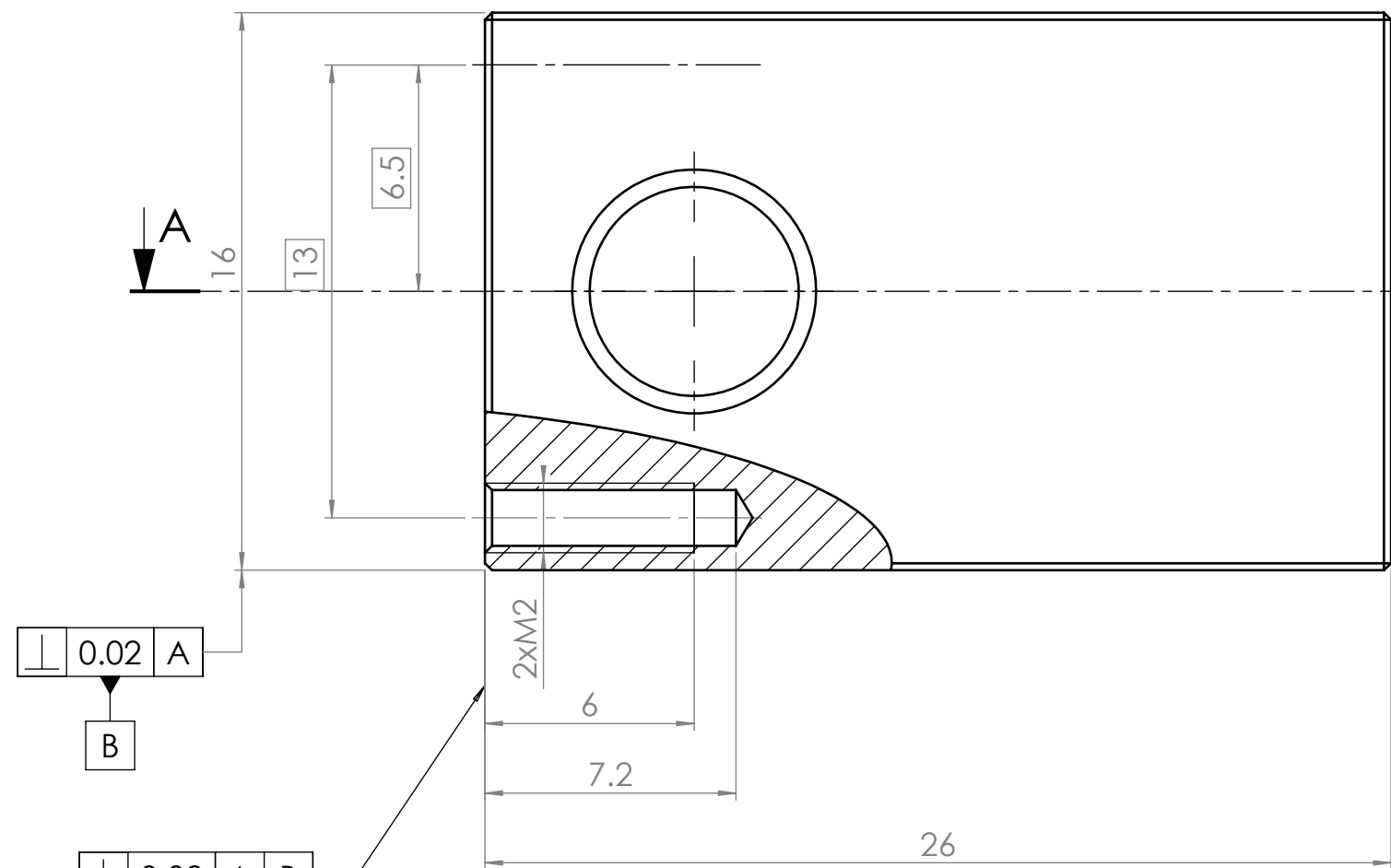
Independence criterion ISO 8015
General tolerances UNI EN 22768-mK

Chamfer 0.2x45°

\sqrt{Ra} 0.8

#	MATERIAL	STUDENT	Build
-			03/04/2019 17:13:35
SUBJECT		COURSE	SCALE 5:1
DESCRIPTION	Front_lower_block		DATE 11/06/2019
 Politecnico di Torino	SURFACE TEXTURE	WEIGHT (Kg)	 
	PAPER A3 1/1	Drawing N.	
Politecnico di Torino - Corso Duca degli Abruzzi, 24 - 10129 TORINO			

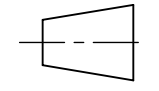
**SolidWorks Educational Edition.
For Instructional Use Only.**



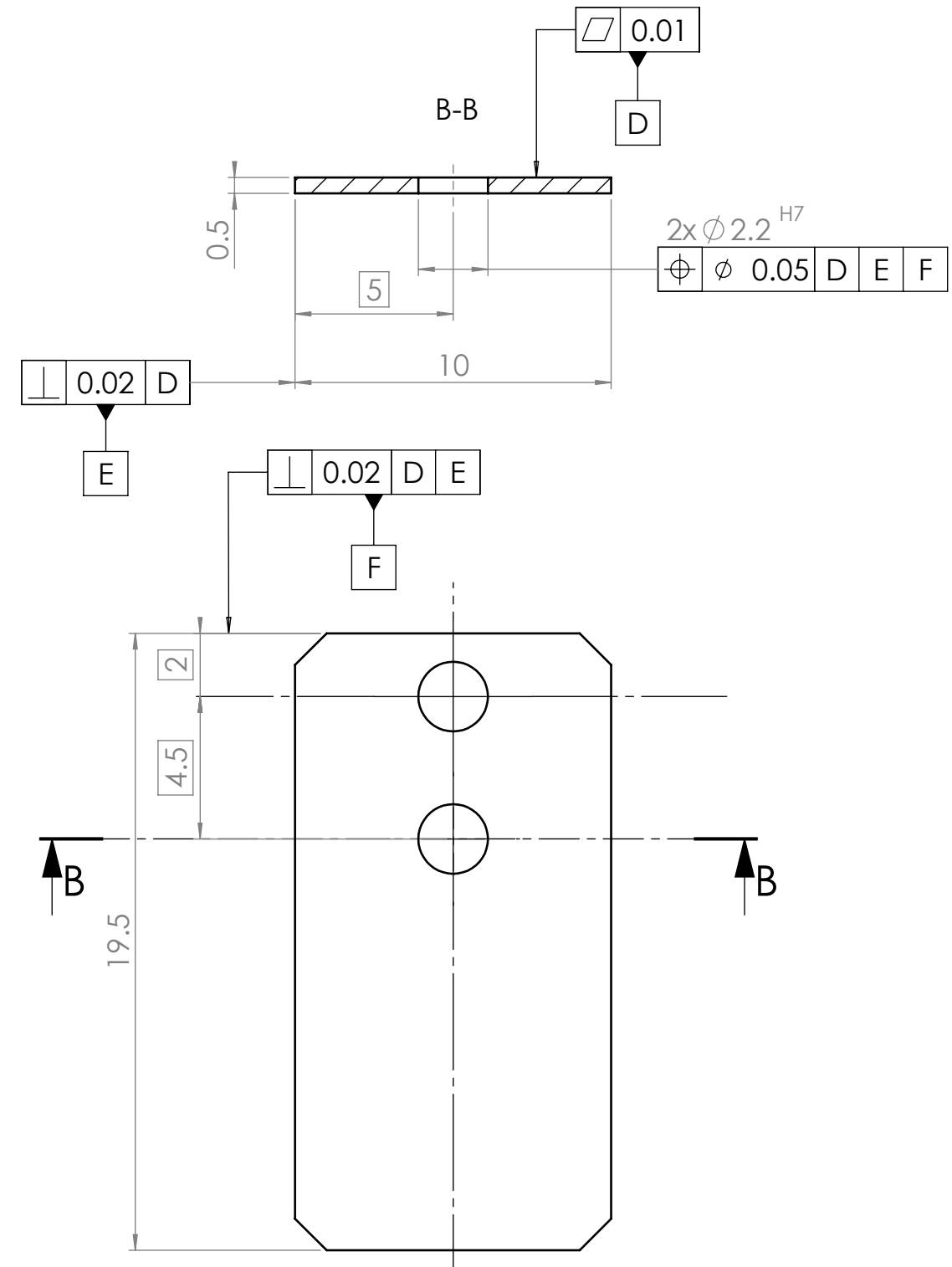
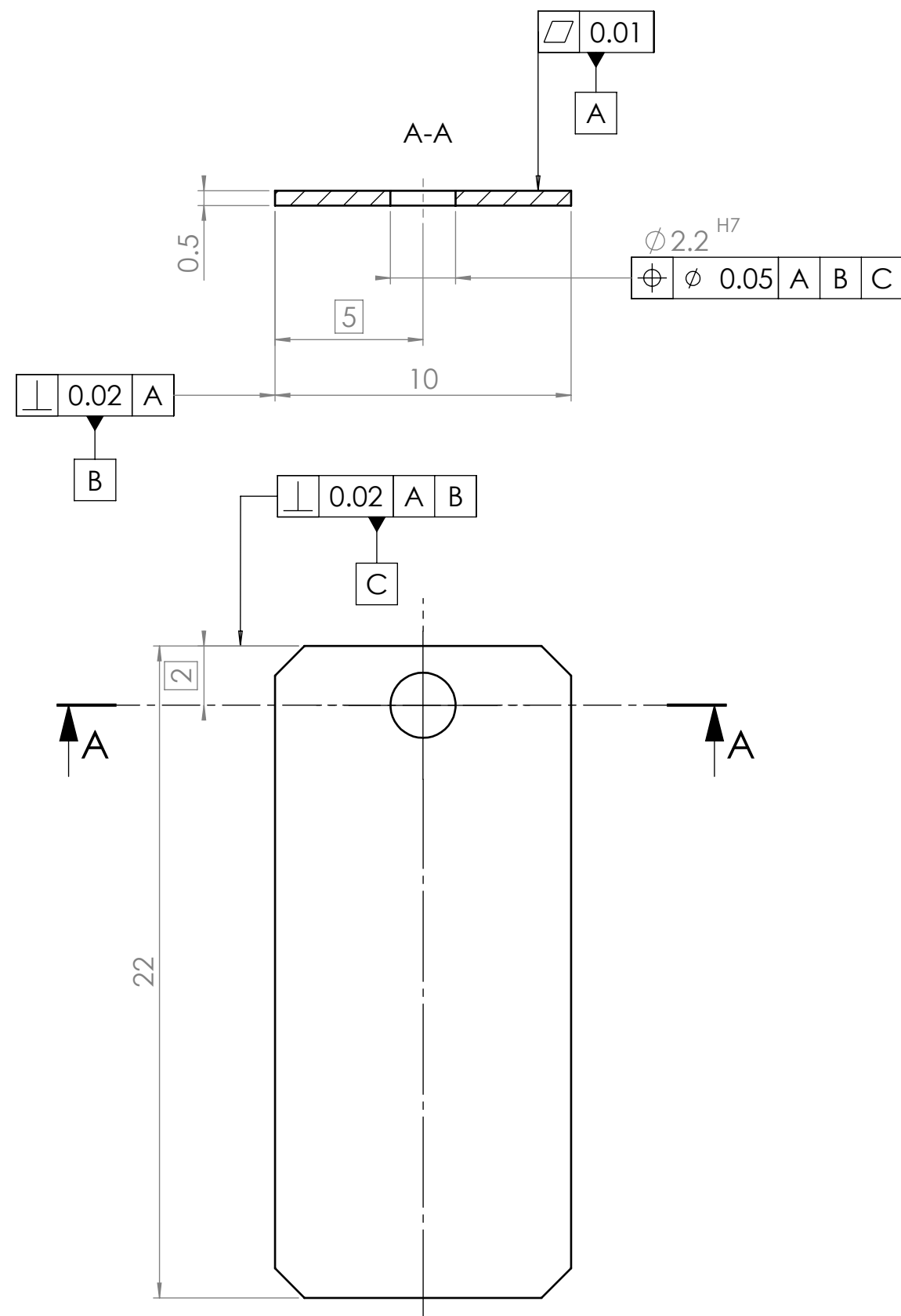
Independence criterion ISO 8015
General tolerances UNI EN 22768-mK

Chamfer 0.2x45°

\sqrt{Ra} 0.8

#	MATERIAL	STUDENT	Build
-			03/04/2019 17:13:35
SUBJECT		COURSE	SCALE 5:1
DESCRIPTION	Rear_lower_block		DATE 11/06/2019
 Politecnico di Torino	SURFACE TEXTURE	WEIGHT (Kg)	 
	PAPER A3 1/1	Drawing N.	
Politecnico di Torino - Corso Duca degli Abruzzi, 24 - 10129 TORINO			

**SolidWorks Educational Edition.
For Instructional Use Only.**



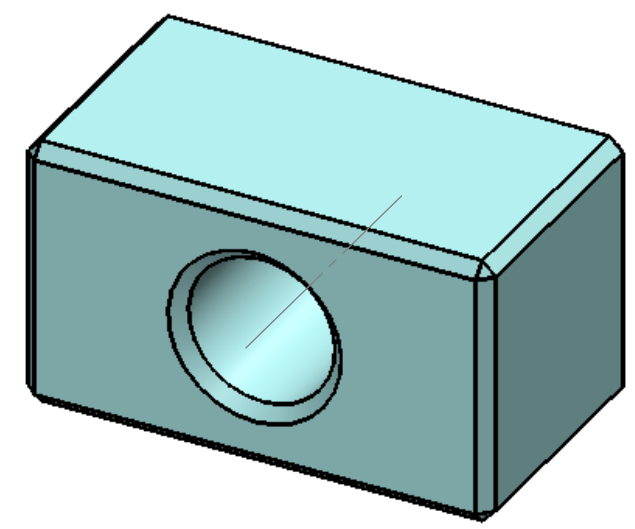
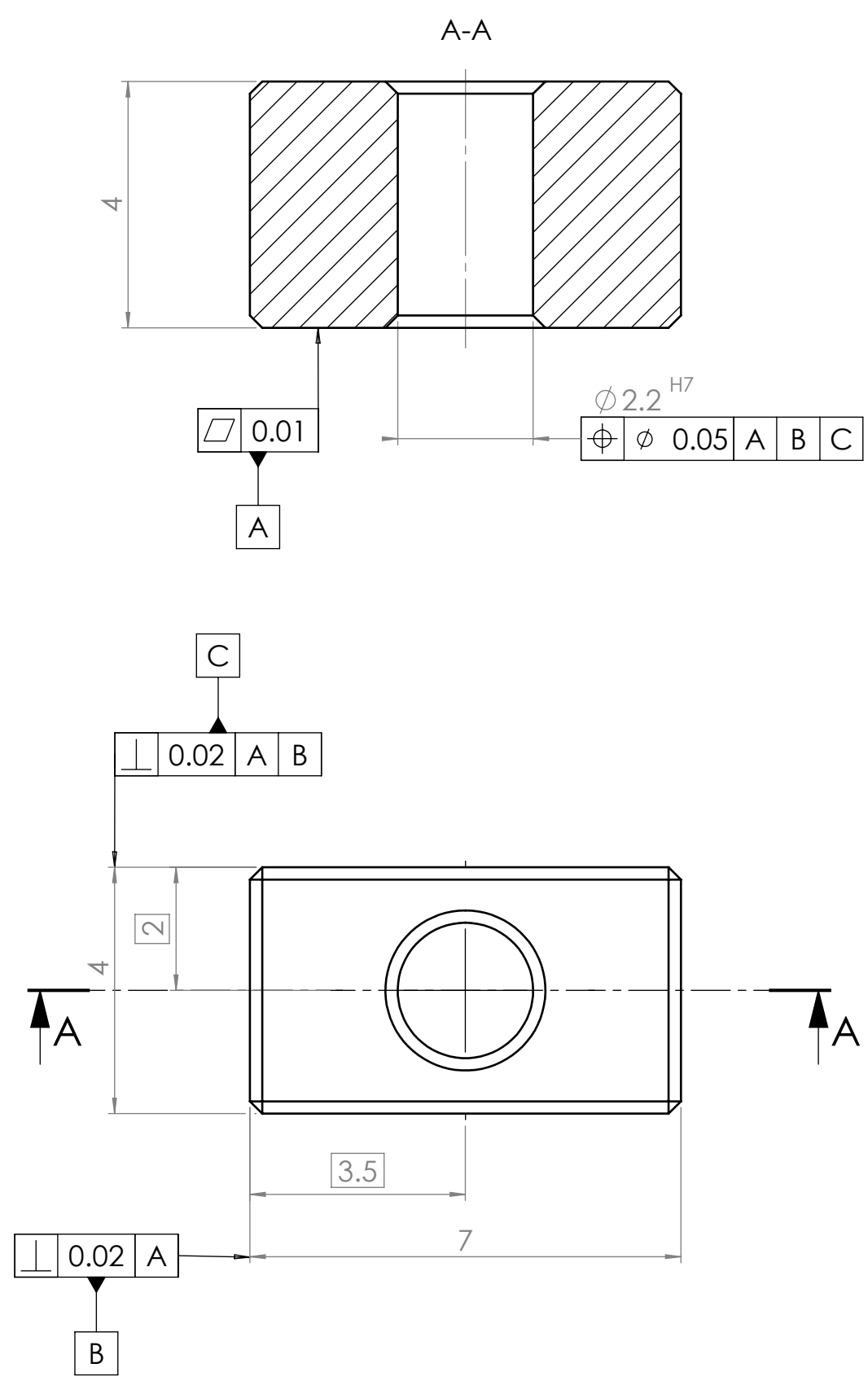
Independence criterion ISO 8015
General tolerances UNI EN 22768-mK

Chamfer 1x45°

Ra 0.8

#	MATERIAL	STUDENT	Build
-			03/04/2019 16:50:34
SUBJECT		COURSE	SCALE 5:1
DESCRIPTION	Vertical_plate		DATE 11/06/2019
 Politecnico di Torino	SURFACE TEXTURE	WEIGHT (Kg)	
	PAPER A3 1/1	Drawing N.	
Politecnico di Torino - Corso Duca degli Abruzzi, 24 - 10129 TORINO			

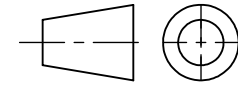
**SolidWorks Educational Edition.
For Instructional Use Only.**



Independence criterion ISO 8015
 General tolerances UNI EN 22768-mK

Chamfer 0.2x45°

\sqrt{Ra} 0.8

#	-	MATERIAL	STUDENT	Build	03/05/2019 14:32:57
SUBJECT			COURSE	SCALE	10:1
DESCRIPTION	Front_higher_block			DATE	11/06/2019
 Politecnico di Torino			SURFACE TEXTURE	WEIGHT (Kg)	
			PAPER	Drawing N.	
Politecnico di Torino - Corso Duca degli Abruzzi, 24 - 10129 TORINO			A3 1/1		

**SolidWorks Educational Edition.
 For Instructional Use Only.**

Reference

- [1] von Helmholtz H.L.F., *On the sensations of tone*, Dover Publications, Inc., New York, 1954. Original edition: *Die Lehre von den Tonempfindungen als physiologische Grundlage für die Theorie der Musik*, Vieweg und Sohn, Braunschweig, 1863.
- [2] Schoonderwaldt E., *Mechanics and acoustics of violin bowing*, Doctoral Thesis, KTH Computer Science and Communication, Stockholm, Sweden, 2009.
- [3] Schelleng J.C., "The bowed string and the player", *J. Acoust. Soc. Am.*, 1973.
- [4] Guettler K., "On the creation of the Helmholtz motion in bowed strings", *Acta Acustica united with Acustica*, 2002.
- [5] Askenfelt A., "Measurement of the bowing parameters in violin playing. II: Bow-bridge distance, dynamic range, and limits of bow force", *J. Acoust. Soc. Am.*, 1989.
- [6] Cronhjort A., "A computer-controlled bowing machine (MUMS)", Speech Trans. Lab. Quarterly Progress and Status Report, KTH, Stockholm, Sweden, 1992.
- [7] Bonisoli E., Delprete C., "Levitron: an exotic toy of nonlinear and linearised dynamics", ICCM2014, Cambridge, 2014.
- [8] Woodhouse J., Galluzzo P. M., "The bowed string as we know it today". *Acustica - Acta Acustica*, 2004.
- [9] Raman C. V., "On the mechanical theory of the vibrations of bowed strings and of musical instruments of the violin family, with experimental verification of the results: Part I", *Indian Assoc. Cultivation Sci. Bull.*, 1918.
- [10] Galluzzo P., "On the playability of stringed instruments", Doctoral dissertation, University of Cambridge, 2004.
- [11] Saunders, F.A. "The mechanical action of violins", *J. Acoust. Soc. Am.* 9, 1937.
- [12] Barnes P., Chandler P.J., Cooke L., Fredin S., Hammel G., Townsend P.D., Whitlow H.J., Wilsen L., "Analysis of sound spectra from bowed violins and violas", *Catgut Acoust. Soc. Newsletter No. 40*, 1983.
- [13] Bradley, J.S., Stewart, T.W.W., "Comparison of violin response curves produced by hand bowing, machine bowing, and an electromagnetic driver", *J. Acoust. Soc. Am.* 48, 1970.
- [14] Coates S.R., Higgs S.J.R., Parsons L.J., Townsend P.D., "Analysis of tones from automatically bowed violins", *Catgut Acoust. Soc. Newsletter No. 24*, 1975.
- [15] Lawergren B., "On the motion of bowed violin strings", *Acustica* 44, 1980.
- [16] Raman, C.V., "Experiments with mechanically-played violins", *Proc. Indian Assoc. for the Cultivation of Sci.* 6, Calcutta, 1920. Reprinted: C.M. Hutchins, ed., *Benchmark Papers in Acoustics, Vol. 5: Musical Acoustics, Part I, Violin Family Components*, Dowden, Hutchinson & Ross, Stroudsburg, PA, 1975.
- [17] Demoucron M., Askenfelt A., Causse R., "Measuring bow force in bowed string performance: Theory and implementation of a bow force sensor", *Acta Acustica united with Acustica*, Hirzel Verlag, 2009.